Endometrial Receptivity Defects and Impaired Implantation in Diabetic NOD Mice 1

Authors: Albaghdadi, Ahmad J.H., and Kan, Frederick W.K.

Source: Biology of Reproduction, 87(2)

Published By: Society for the Study of Reproduction

URL: https://doi.org/10.1095/biolreprod.112.100016

BIOLOGY OF REPRODUCTION (2012) **87**(2):30, 1–16
Published online before print 25 April 2012.
DOI 10.1095/biolreprod.112.100016

Endometrial Receptivity Defects and Impaired Implantation in Diabetic NOD Mice[1]

Ahmad J.H. Albaghdadi and Frederick W.K. Kan[2]

Department of Biomedical and Molecular Sciences, Queen's University, Kingston, Ontario, Canada

ABSTRACT

Implantation failure is a major hurdle to a successful pregnancy. The high rate of postimplantation fetal loss in nonobese diabetic (NOD) mice is believed to be related to an abnormal decidual production of interferon (IFN)gamma. To address whether diabetes alters the natural events associated with successful implantation, certain morphological and molecular features of uterine receptivity in diabetic NOD (dNOD) mice were examined in normally mated pregnancy and in concanavalin A (ConA)-induced pseudopregnancy. As opposed to normoglycemic NOD (cNOD) mice, dNOD mice expressed retarded maturation of their uterine pinopodes and overexpressed MUC1 mucin at implantation sites ($P < 0.001$). Uterine production of leukemia inhibitory factor (LIF) and phosphorylation of uterine NFkappaBp65 and STAT3-Ty705 were found to be low ($P < 0.01$) during Day 4.5 postcoitum, whereas IFNgamma was aberrantly overexpressed. Loss of temporal regulation of progesterone receptor A (PR A) and PR B, together with aberrantly increased expression of the protein inhibitor of activated STAT-γ (PIASγ) ($P < 0.01$) and reduced recruitment ($P < 0.01$) of the latter to nuclear progesterone receptor sites were prominent features of decidualization failure occurring at peri-implantation in dNOD mice. In conclusion, the aberrant expression of endometrial IFNgamma in dNOD mice is associated with a nonreceptive endometrial milieu contributing to peri-implantation embryo loss in type 1 diabetes.

IFNγ, implantation failure in type 1 diabetes, MUC1, NFκB, NOD mice, PIASγ, progesterone receptor, STAT3, uterodomes

INTRODUCTION

Diabetic women are ninefold more likely to experience fetal loss after implantation [1, 2]. The exact mechanism contributing to early pregnancy failure and recurrent spontaneous abortion in autoimmune diabetes remains largely unknown. In the nonobese diabetic (NOD) mouse model of human type 1 diabetes, an inherited autoimmune activation of a subset of T cells is believed to result in the induction of an interferon-γ (IFNγ)-mediated embryo-lethal T helper type1 (Th-1) local uterine cytotoxicity during midgestation that is widely considered central to pregnancy failure in women with diabetes [3]. Although the quality of the blastocyst is important for implantation, early pregnancy progression in women and mice requires the induction of highly programmed and temporally restrained successions of cellular events that define the time at which the uterus is maximally receptive and is termed the ''window of implantation'' (WOI) [4, 5]. In the mouse, generation of the receptive uterus reportedly occurs around Day 4.5 postcoitum [6] and is characterized by the development of certain specific transformational changes in both uterine epithelium and stromal cells, occurring at the molecular level [4–7]. Of the latter, the formation of apical, epithelial, ectoplasmic projections, which are termed uterodomes (pinopodes) [4, 5], are essential for the establishment of an initial physical interaction between the trophoectoderm of the blastocyst and the ''transformed'' uterine epithelium during the attachment phase of the implantation cascade [6, 7]. The formation and maturation of uterodomes are mechanistically linked to increased phosphorylation and nuclear translocation of the transcriptional factors NFκBp65 and STAT3 in the implantation site epithelium [8, 9]. The induction of phosphorylation of uterine NFκBp65 and STAT3 is believed to be the outcome of a nidatory estrogen and is mediated through the local actions of growth factors and cytokines, such as leukemia inhibitory factor (LIF) and interleukin1 (IL1) during implantation [10]. Notably, it has been established that high levels of IFNγ are detrimental to LIF-induced nidatory changes in uterine cells [11] and that pathologically increased expression of IFNγ in decidua is consistently observed in diabetic women experiencing recurrent spontaneous abortion [12].

Of the molecular mechanisms that are critical for both human and murine uterine receptivity is the strict, timely inhibition of epithelial MUC1 expression [13]. MUC1 is a large (mass >250 kDa) type 1, or single-pass, cell surface-associated glycoprotein that is believed to constitute approximately 10% of the total glycoprotein content of the apical cellular glycocalyx, which extends a considerable distance of 200–500 nm into the lumen of the uterus (reviewed in references 14 and 15]. It is believed that MUC1 provides the uterine epithelium with lubrication and protection against bacterial and proteolytic attacks [14, 15]. Importantly, MUC1 is thought to cause a steric hindrance that masks the expression of cell adhesion molecules, such as integrins and selectins, which are critically involved in the attachment phase of human and murine blastocyst implantation [13–16]. It has been hypothesized that transcriptional and translational loss of MUC1 occurring at the surface of uterodomes is vital for supplying a MUC1-free zone for embryo-endometrial interactions during implantation in humans [17]. However, this strict, timely loss of apical epithelial mucin MUC1 expression from implantation sites in mice and women [13, 16] suggests that dysregulation of the mechanisms involved in down-regulating the expression of MUC1 at the time of implantation may prevent implantation and the establishment of early pregnancy in these two mammalian species.

During early pregnancy, the decidualization of uterine stromal cells that occurs in response to the implanting embryo facilitates peri-implantation embryonic development [18]. Th-1 cytokine-mediated disruption of the implantation process results in early termination of pregnancy and subsequent infertility in nondiabetic mice [12, 18, 19]. However, normal

[1]Supported by a grant from Canadian Institutes of Health Research (CIHR) to F.W.K.K.
[2]Correspondence: E-mail: kanfwk@queensu.ca

Received: 18 February 2012.
First decision: 6 March 2012.
Accepted: 20 April 2012.

eISSN: 1529-7268 http://www.biolreprod.org
ISSN: 0006-3363

levels of expression of inflammatory cytokines are believed to be crucial for establishing early pregnancy in mice and women [12, 18]. Of particular interest are certain molecular interactions occurring at the nuclear progesterone receptors (PR) involving recruitment of IFNγ-inducible protein inhibitors of activated STAT-y (PIASy), which are believed to regulate some PR-mediated transcriptional activities involved in murine and human implantation, namely, uterine MUC1 expression and stromal decidualization in vitro [20–22]. It remains unclear whether decidualization failure in the endometrium of diabetic women who are experiencing recurrent spontaneous abortions is related to locally high resistance to progesterone signaling during embryo implantation. We hypothesized that early pregnancy failure in autoimmune diabetic subjects is likely a consequence of the nonreceptive uterine milieu of uterodome maturation failure, poor decidualization, and aberrant expression of the anti-implantation mucin MUC1 during implantation. Results obtained in the present study suggest a detrimental role for abnormally expressed uterine IFNγ and/or its downstream PIASy-mediated suppression of implantation in diabetic NOD (dNOD) mice. The present investigation also characterized certain aspects of implantation, both morphologically and molecularly, in normally mated and concavalin A (ConA)-induced pseudopregnancy in dNOD mice on Days 4.5 and 6.5 postcoitum, respectively.

MATERIALS AND METHODS

Animal Models and Experimental Design

All animal procedures and protocols were approved by the University Animal Care Committee of Queen's University. A total of 110 female NOD/ShiLtJ and 25 female BALB/c mice were purchased from Jackson Laboratory at the age of 7 weeks. An Ultra glucometer (Accu-Chek Aviva/Roche Diagnostic) was used to monitor changes in blood glucose of all mice through tail venipuncture once per week beginning at the age of 7 weeks, during pregnancy, and at the point they were euthanized. Single drops of freshly obtained tail vein blood were sufficient to accurately measure blood glucose in all mice. Animals having nonfasting blood glucose concentrations of $\geq$14.9 mMol/L were considered diabetic and were annotated as dNOD mice. All normoglycemic mice with nonfasting blood glucose concentrations of $\leq$10.0 mMol/L were referred to as normoglycemic NOD (cNOD) mice. Control BALB/c mice were used to further monitor changes in cNOD mice and to exclude the possibility of strain-related immune defects in NOD mice on our interpretation of the selected endometrial and/or decidual biomarkers of dNOD mice (data not shown). A number of animals (n = 5) of the cNOD and dNOD groups were allowed to carry to term and were monitored for changes in their blood glucose levels throughout pregnancy and 10 days postpartum, as described in the supplementary data (Supplemental Fig. S1 available online at www.biolreprod.org). Except during normal mating and induction of pseudopregnancy, all mice were individually housed at ambient temperatures in 12D:12L cycles and ad libitum access to a 20% fortified protein pellet diet (Co-op Feeds) and tap water.

Preparation of Pregnant and Pseudopregnant Bead-Induced Deciduoma Decidual Samples

Peri-implantation (Gestational Day 4.5 [E4.5]; n = 37–45) and post-implantation (E6.5; n = 39–41) pregnant and/or pseudopregnant (E4.5 bead-induced deciduoma [bid] and E6.5bid; n = 5/group per experiment) mouse uteri were prepared after mice were mated with fertile or vasectomized males, as previously described [23]. The morning on which a vaginal plug could be detected was considered E0.5. Based on the rationale that the presence of an embryo is not required for the initiation of decidualization in mice [23] and in order to assess the responsiveness of the endometrium in dNOD to deciduogenic signals in the absence of an embryo, we examined uteri of dNOD mice in response to intrauterine-injected ConA beads as the best-described agent for artificially inducing decidualization in mice [23]. On average, 15 blastocyst-sized ConA-coated Sepharose beads (Sepharose-conjugated [45–156 μm]; Sigma-Aldrich) were injected into the lumen of the left uterine horn of anesthetized animals between 1300 and 1600 h on Day 2.5 of pseudopregnancy, in accordance with the previously described procedure [23].

Animal Sacrifice and Sample Collection

Anesthetized (ketamine-xylazine) pregnant and pseudopregnant mice were euthanized on the mornings of Days 4.5 and 6.5 of their respective pregnancies, by cardiac puncture, between 0900 and 1100 h. Collected blood samples were left to stand at room temperature for 1 h before isolation of their serum, which were stored at −80°C until analyzed for progesterone and estradiol (data not shown) by radioimmunoassay, conducted at the Department of Clinical Chemistry (Kingston General Hospital, Kingston, Ontario, Canada). Serum samples from pregnancy Day 8.5 were also collected and measured for progesterone and estrogen levels (data not shown) to validate differences observed in the concentration of these two hormones during early pregnancy in dNOD mice. Ovaries, oviducts, and uteri were carefully dissected from the carcasses and placed in ice-cold PBS in Petri dishes. Using a dissecting microscope, we carefully trimmed all mesenteric fat from uteri, which were immediately weighed. The numbers of corpora lutea and implantation sites (viable and resorbed) were counted from E4.5 and E6.5 pregnant mouse ovaries and uteri, respectively. For protein and/or RNA extraction, segments of uterine horns containing interimplantation sites of pregnant and pseudopregnant mice were transected and stored in liquid nitrogen. For RNA-targeted applications, decidual samples were stored in an RNA-stabilizing buffer (RNAlater RNA stabilization reagent; Qiagen).

Morphological Analysis and Implantation Site Count

Assessment of the uterine external morphological features in pregnant mice, including counts of implantation sites and photography, were performed using a computerized dissecting microscope (Leica diagnostic instruments) and image acquisition and analytic software (SPOT version 2.2.0). The percentage of peri-implantation embryo loss was calculated as described by Bindali and Kaliwal [24], using the formula: percentage of peri-implantation loss = (total number of corpora lutea − total number of implantations/total number of corpora lutea) × 100%. The mean percentage ± SEM of postimplantation embryo loss was calculated by (total number of resorbed implantation sites per dam/total number of implantation sites per dam) × 100%.

Antibodies

A hamster polyclonal antibody (code CT2) recognizing the highly conserved domain SSLSYTNPAVAATSANL of the cytoplasmic tail region of human MUC1 was generously provided by Dr. Sandra Gendler (Mayo Clinic, Scottsdale, AZ). Texas Red-goat anti-Armenian hamster antibody (code SC-2997; Santa Cruz Biotechnology) was used for immunofluorescence detection of MUC1. An HPLC-purified (95%) synthetic peptide (SSLSYTNPAVAAT-SANL) (Sheldon Biotechnology Center) was used to neutralize CT2 antiserum in preparation of MUC1 control sections. Rabbit polyclonal anti-NFκBp65 (code C-100-4165; Rockland Immunochemicals), rabbit polyclonal anti-phospho-(Ser 536)-NFκBp65 (code SC-33020; Santa Cruz Biotechnology), and rabbit polyclonal anti-STAT3 and rabbit polyclonal anti-phospho-(Tyr705)-STAT3 antibodies (Cell Signaling Technology) were used to examine NFκBp65 and STAT3 expression and phosphorylation, respectively. Rabbit polyclonal anti-PR (code C-19; Santa Cruz Biotechnology) and mouse monoclonal anti-PIASy (code C-11; Santa Cruz Biotechnology), and their immunofluorescent-conjugated isotype control antibodies (Santa Cruz Biotechnology) were used in Western Blot (WB) and in immunofluorescence analyses, respectively. Bovine Texas Red-conjugated goat-anti-rabbit (immunoglobulin G [IgG]; Santa Cruz Biotechnology) and AlexaFluor 488-conjugated goat anti-mouse antibodies were applied for double-immunofluorescence detection and colocalization of PR and PIASy, respectively. Biotinylated monoclonal anti-IFNγ (clone 1-D1K 1-biotin; Mabtech Inc.) was used for immunohistochemical detection of IFNγ in histological sections. Isotype anti-mouse IgG was substituted for anti-IFNγ antibody in control sections.

MUC1 and INFγ Immunohistochemistry

Following standard procedures for immunohistochemical labeling of deparaffinized tissue sections [25], over 100 methacarn-fixed (60% methanol, 30% chloroform, and 10% acetic acid) paraffin-embedded serial (5-μm-thick) sections of uterine and decidual samples from cNOD and dNOD mice were probed for either MUC1 or IFNγ. Five implantation and interimplantation sites from cNOD mice on E4.5 and E6.5 of pregnancy (n = 7/group) and dNOD (n = 10 /group) mice were examined by two independent investigators. Texas Red-conjugated goat anti-Armenian hamster antibody (0.8 mg/ml) was used for

TABLE 1. Primers used for real-time (quantitative) and/or semiquantitative PCR detection of IFNγ, MUC1, and GAPDH.

Gene	GenBank accession no.	Sense primers	Antisense primers	Product size (bp)	Annealing temperature (°C)
IFNγ	NM_008337	5′-GCTTTAACAGCAGGCCAGAC-3′	5′-GGAAGCACCAGGTGTCAAGT-3′	100	60.02
MUC1	NM_013605	5′-GTGAGCCAGGACTTCTGGTAG-3′	5′-CAGGCCAGTCCTTCTGAGAG-3′	131	58.9
GAPDH	NM_001473623	5′-GTGTCCGTCGTGGATCTGA-3′	5′-CCTGCTTCACCACCTTCTTG-3′	76	60.71

indirect immunofluorescence detection of MUC1, whereas localization of IFNγ in labeled uterine sections was visualized with 3,3-diaminobenzidine tetrahydrochloride (DAB) substrate (Zymed Laboratories Inc.). Nuclei were counterstained with either 4′,6-diamidino-2-phenylindole (DAPI) for immunofluorescence detection of MUC1 or with Meyer hematoxylin (Sigma-Aldrich) in IFNγ-labeled sections. A fluorescent mounting medium (Dackocytomation or Histomount; (Zymed Laboratories Inc.) was used in the final preparation of labeled sections. MUC1 control sections were incubated overnight at 4°C with neutralized CT2 anti-MUC1 antiserum as described earlier. Horseradish peroxidase-conjugated anti-mouse IgG was used as a substitute for IFNγ in control immunohistochemical staining.

Immunofluorescent Detection and Colocalization of Uterine PIASy and Nuclear PR

Immunofluorescence detection and colocalization of PIASy and nuclear PR were performed with methacarn-fixed paraffin-embedded uterine sections prepared from pregnant and pseudopregnant mice at E4.5 and E6.5, respectively, according to standard protocol [25]. Briefly, dewaxed and rehydrated sections were incubated in a dark humidified chamber for 1 h at room temperature in a blocking solution containing 5% fetal calf serum in PBS containing 0.05% Tween-20 (PBST). Incubation with the anti-PR antibody was carried out at 4°C overnight, after which uterine sections were rinsed twice in PBS for 5 min before they were incubated for 45 min at room temperature with Texas Red-conjugated goat-anti-rabbit antibody. After a brief rinse of sections in PBST, each for 5 min, the immunohistochemical labeling for PIASy was attempted in a manner similar to that described above for PR, using PIASy-specific antibodies described earlier. Nuclei were counterstained with DAPI, and fluorescence emission and colocalization in immunolabeled uterine sections were analyzed using an inverted laser-scanning confocal microscope (Leica model SP2 AOBS). Pixel intensities of yellow fluorescence, which represented the percentage of colocalization of green (PIASy) and red (PR) fluorescent signals in overlaid images, were quantitatively calculated by intensity correlation analysis using ImageJ analytic software (National Institutes of Health; http://rsb.info.nih.gov/ij). For controls, anti-PR and anti-PIASy antibodies were replaced with respective isotype control anti-mouse IgGs (Santa Cruz Biotechnology) at the same dilution. Intensities of nonspecific fluorescence obtained in isotype control-stained uterine sections were subtracted from data obtained in positively stained uterine sections. Pearson correlation coefficients close to 1 were indicative of a reliable colocalization [26].

Scanning and Transmission Electron Microscopy

Scanning and transmission electron microscope examinations were performed to assess morphological features of uterine receptivity in the implantation sites of tissues obtained from cNOD and dNOD mice according to a standard protocol [27]. Implantation site specimens were fixed in 2.5% glutaraldehyde (in PBS) and postfixed for 1 h at room temperature in 1% aqueous osmium tetroxide. For scanning electron microscopy (SEM), samples were dehydrated in a graded series of ethanol solutions, critical-point dried, mounted, coated with gold in a sputter coater (Cressington-108 Auto fine coater), and examined with a Hitachi (model S-3400N) scanning electron microscope, and images were digitally recorded. For transmission electron microscopy (TEM), samples were fixed as described above, processed, and embedded in epoxy resin (Epon) according to a standard protocol [27]. Ultrathin (1-μm-thick) sections were prepared from selected regions of epoxy-embedded implantation sites and counterstained for 10 min with 4% aqueous uranyl acetate, followed by 2 min of treatment with lead citrate, and viewed with a Hitachi model 7000 transmission electron microscope operated at 75 kV

Preparation of Uterine Cytosolic and Nuclear Extracts

Uterine samples collected from mated normoglycemic and dNOD mice were homogenized in homogenization buffer (cytosolic and nuclear extraction buffer kit; Biovision Inc.) using an ice-cold, sterile glass Dounce-tissue homogenizer. Separation of the cytoplasmic and the nuclear fractions was performed according to the manufacturer's instructions. The protein concentration of each fraction was determined by the Bradford assay. Samples were stored at −80°C until further analysis. Nuclear protein fractions were used to detect the phosphorylated proteins NFκBp65 and STAT3.

SDS-PAGE and Western Blot Analysis

Mouse uterine cytosolic and nuclear proteins were resolved on 6% or 8% (w/v) Tris-SDS denaturing polyacrylamide gels (containing 8 M Urea) in 1× sample loading buffer (150 mM sodium chloride, 1.0% Triton X-100, and 50 mM Tris, pH 8.0). Protein samples were transferred to polyvinylidene fluoride membranes, and blots were probed with the appropriate antibodies, followed by signal detection using Western heightening-enhanced chemiluminescence advanced chemiluminescence substrate (PerkinElmer Inc.) and exposure on X-Omat Blue film (PerkinElmer Inc.). Background-corrected intensities of Western blot protein bands on scanned films were processed using Image J software. Data were expressed as means ± SEM. GAPDH (detected as a band at 37 kDa) was the internal loading control.

Primers, RNA Extraction, and Gene Expression Analysis

Table 1 summarizes the primers used in the present study. Primers for IFNγ (GenBank accession no. NM_008337) and those for MUC1 (GenBank accession no. NM_013605) cytoplasmic tail region were designed using Oligo-Calculator version 3.23 software [28] and were cross-checked for specificity through GenBank/NCBI and/or online FASTA sequence comparison resources (FASTA Sequence Comparison at the University of Virginia; http://fasta.bioch.virginia.edu) and the Washington University Basic Local Alignment Search tool (WU-BLAST; http://www.ebi.ac.uk/Tools/sss/wublast/nucleotide.html). RNeasy mini-kits (Qiagen) and silica-membrane RNeasy spin columns (Qiagen) were used to prepare total RNA from frozen uterine samples of nulliparous and pregnant mice according to the manufacturer's instructions. Total RNA (2 μg) was treated with DNase (1 $U \cdot ml^{-1}$) and reverse transcribed using a first-strand complementary DNA synthesis kit (Qiagen). Quantitative-PCR assays were carried out in triplicate with equal aliquots of cDNA (2 μl), using the Rotor Gene 3000 instrument (Corbet Real Time PCR) and iTaq Fast SYBR Green Supermix with the reference dye ROX (Bio-Rad Laboratories Ltd.) in a 20-μl reaction volume. The relative expression level (*R*) and fold change in MUC1 gene expression were calculated using the comparative threshold cycle ($\Delta\Delta C_T$) method with normalization to that of GAPDH. *R* values were measured as the negative values of $\Delta\Delta C_T$ as exponent of 2 according to the equation: $R = 2^{\wedge(-\Delta\Delta C_T)}$ where $\Delta\Delta C_T = \Delta C_T$ (Target) − ΔC_T (Endogenous Control) [29]. IFNγ mRNA expression was also examined with a conventional semiquantitative PCR assay using equal amounts of mRNA and iTaq-DNA polymerase (Qiagen). A revised transcribed complementary DNA obtained from lipopolysaccharides-stimulated mouse peritoneal cells (generously provided by Dr. Myron R. Szewczuk, Queen's University, Kingston, Ontario, Canada) and the IFNγ complementary sense sequence ''GTCTGGCCTGCTGTTAAAGC'' (ACGT-DNA Technologies Corp.) were used for the positive and negative control detection of murine IFNγ, respectively. Nucleotide sequences of amplicons generated by qPCR and/or semiquantitative PCR were confirmed by ACGT-DNA Technologies.

Measurements and Statistical Methods

To investigate the association between uterine MUC1 mRNA expression and the degree of colocalization of PIASy and PR (represented as the percentage of Pearson correlation coefficient in double-immunofluorescence assays), scatter plots were prepared for all datasets of cNOD and dNOD dams during early pregnancy and pseudopregnancy. Linear regression analyses were performed to determine the slope for the best-fit line in each data set, and Spearman correlation coefficients were calculated. In Western blot analyses, signal intensities of detected protein bands were measured using Image J software. All data are means ± SEM and were analyzed with Graph-Pad Prism

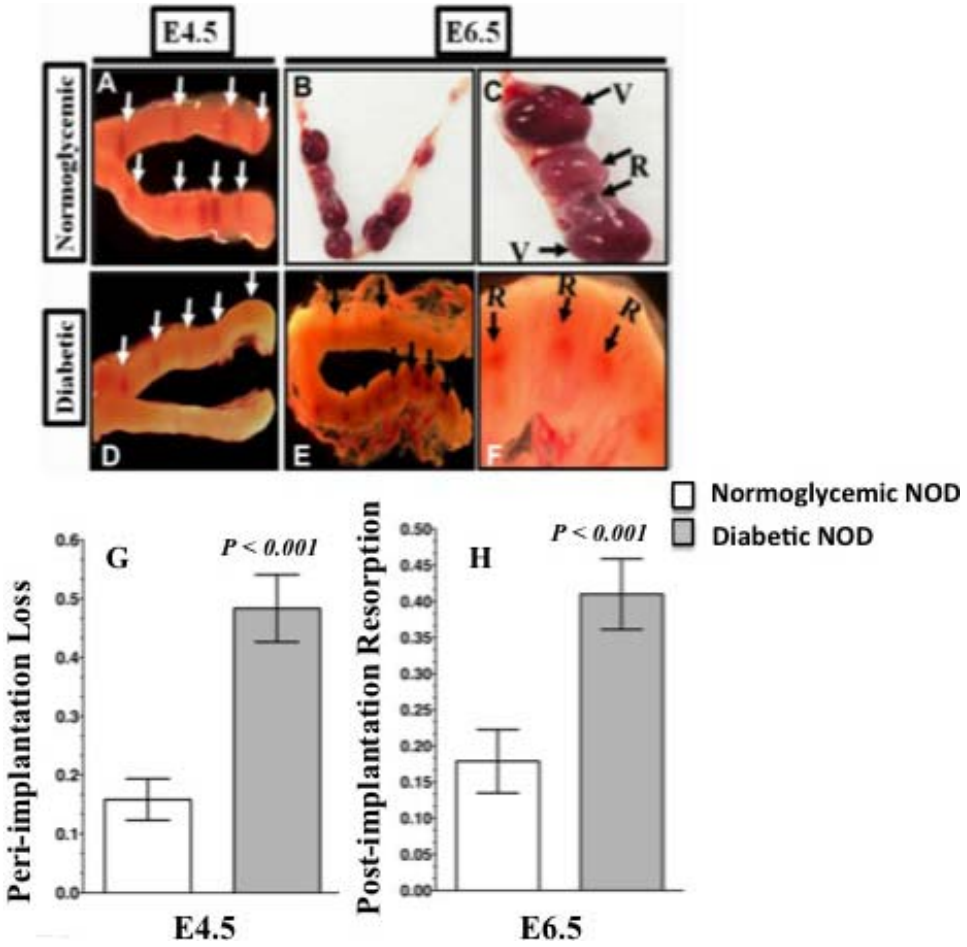

FIG. 1. External morphology of cNOD (**A**–**C**) and dNOD (**D**–**F**) implantation sites during peri- and postimplantation as visualized with a transillumination dissecting light microscope. Data are means ± SEM of peri-implantation embryo loss (**G**) and percentage of postimplantation resorption (**H**). A relative scarcity of implantation sites (**D**, white arrows), significantly higher incidence ($P < 0.001$, n = 11–14) of peri-implantation loss (0.49 ± 0.09 versus 0.17 ± 0.05), and a higher resorption rate ($P < 0.001$, n = 10–12) at postimplantation (0.42 ± 0.07 versus 0.16 ± 0.09) characterized early pregnancy in dNOD mice. **C** and **F**) Higher magnification of typically observed differences in external appearance of implantation sites at E6.5 in cNOD and dNOD dams, respectively. Resorption sites were identified by virtue of their small size and their reduced vascularity in cNOD mice (**B**–**C**; compare viable implantation sites, "V," versus those resorbed, "R"). Note the grayish-brown discoloration distinguishing resorbed postimplantation sites in the overtly diabetic dNOD dams (**E**–**F**, "R" and black arrows). Original magnifications ×8 (**A**, **D**, **E**), ×6.3 (**B**), ×25 (**C**), and ×40 (**F**).

5 software. Significant differences among groups of mice were examined with one-way ANOVA followed by Bonferroni modified post hoc *t*-tests with 95% confidence intervals. Independent one-tailed Student *t*-tests were used to examine differences in peri-implantation loss and percentage of resorption among pregnant NOD groups.

RESULTS

Morphological Features of Early Pregnancy in dNOD Mice

The impact of diabetes on peri- and postimplantation development of pregnant uteri in NOD mice was first assessed morphologically. Overly diabetic dNOD mice had significantly fewer implantation sites on E4.5 than cNOD mice (Fig. 1, compare A with D and the bar graphs in G and Tables 2 and 3) and a significantly higher rate ($P < 0.001$) of embryo resorption at E6.5 (Fig. 1, compare B and C with E and F and the bar graphs in H, and Tables 2 and 3). Under normal circumstances, successful implantation in the mouse leads to a subsequent localized decidualization of the adjacent endometrial stroma, causing enlargement of the uterine segment and an increased endometrial vascular permeability at implantation sites [23]. The first macroscopically visible evidence of successful implantation was localized hypervascularity that could be visualized through a transmitted beam of light passing through the uterine body placed against a dark background. Therefore, in the uteri of cNOD mice at E4.5 and E6.5, embryo

TABLE 2. Percentage of peri-implantation embryonic loss in cNOD and dNOD mice on E4.5.

Mice	Total no. of implantations	Mean no. of implantation sites[a]	Mean corpora leuta[a]	Peri-implantation loss[a]	No. of dams	CI
cNOD	97	9.7 ± 1.11	12.3 ± 1.16	0.17 ± 0.053	11	0.0013
dNOD	74	4.9 ± 1.7*	0.51 ± 0.08*	0.49 ± 0.091*	14	0.0021*

[a] Data are means ± SEM.
* $P < 0.001$ compared to cNOD mice.

TABLE 3. Percentage of resorption of postimplantation embryos in cNOD and dNOD mice on E6.5.

Mice	Total no. of implantations	Mean implantation sites[a]	Total no. of viable implantation	Total no. of resorbed implantation	Resorption[a]	No. of dams	CI
cNOD	105	9.1 ± 0.51	88	17	0.16 ± 0.091	10	0.0011
dNOD	70	5.1 ± 0.096	41	29*	0.42 ± 0.077*	12	0.0037*

[a] Data are means ± SEM.
* $P < 0.001$ compared to cNOD mice.

implantation and postimplantation sites were identified by virtue of their characteristic beaded appearance and their vascular red color as observed through a dissecting microscope (Fig. 1, A and D). Resorbed postimplantation sites were identified by their relatively smaller size and their decreased vascular appearance compared to viable implantation sites in cNOD mice (Fig. 1, B and C). However, resorption among E6.5 implantation sites in dNOD mice was identified by virtue of its relatively smaller size and characteristic brownish discoloration (Fig. 1, E, F, and G). Consistent with decidualization failure in normally mated dNOD mice, uterine wet weight was significantly lower ($P < 0.05$) in the dNOD at E4.5, E6.5, E4.5bid and E6.5bid, respectively (Supplemental Fig. S2). Morphometric analysis of decidualized uterine cross-sectional regions also revealed significantly smaller deciduomas in the uteri of normally mated and ConA-pseduopregnant dNOD mice ($P = 0.0015$; average surface area of 158.3 ± 65 mm^2 compared to an average decidualized area of 388.3 ± 70.1 mm^2 in the cNOD at E4.5bid, n = 5; see Supplemental Fig. S3).

Ultrastructural Features of Implantation Sites in dNOD Mice

To morphologically assess uterine receptivity in dNOD mice, we compared the ultrastructural features of implantation sites prepared from the uteri of dNOD mice at E4.5 to those observed in cNOD mice. Among the alterations in the surface epithelium of the mammalian endometrium in preparation for implantation is the formation of uterodomes or pinopodes [5, 6]. Based on their morphological appearance that reflects the stages of their development, uterodome stages are classified as developing, developed (mature), or regressing [5]. Accordingly, particular attention was paid to the morphology of these structures in our electron micrscopy study. In Figure 2A, a low magnification SEM image revealed a relatively high density of mature uterodomes with characteristically large, dome-shaped terminal ends developing at implantation sites in cNOD; this is best illustrated at the higher magnification shown in Figure 2, B and C. However, the surface topography of the uteri of dNOD mice showed a morphological appearance that was different from these structures. Figure 2D shows a low magnification SEM image of the luminal surface of the uterus of a representative dNOD mouse at E4.5. There appears to be a reduced number of mature uterodomes, as shown by patches of luminal surface dominated by underdeveloped or immature microvilli (Fig. 2E). Importantly, the absence of well-developed uterodomes at the implantation site luminal epithelium coincides with delayed implantation at E4.5 (Fig. 2F) and reduced uterine expression of LIF (see Supplemental Fig. S4) in the diabetic mice.

In rodents, uterodome maturation has been linked to structural alterations in the apical and lateral plasma membranes in uterine cells. The reduced expression of apical cell surface glycoproteins and the structural downregulation of lateral junctional complexes, such as tight junctions, adherens junctions, and desmosomes, have been linked to successful implantation reaction in mammalian uterine epithelium [7]. Therefore, we further assessed uterodome maturation in dNOD mice by using TEM. As shown in Figure 3, A and B, implantation sites obtained from cNOD mice revealed that mature uterodomes exhibited a relatively glycocalyx-free cell surface and were associated with features suggestive of increased secretory activity, such as the relative abundance of Golgi complexes and outbursts of secretory materials (Fig. 3, A and B). Unpredictably, the sparsely distributed and partially developed uterodomes in dNOD mice at E4.5 were coated with a relatively thick layer of glycocalyx, frequently harbored intercellular clefts or blebs on their lateral plasma membranes, and contained many lipid droplets accompanied by the frequent presence of inclusion bodies (Fig. 3, C and D).

Uterine MUC1 Expression in dNOD Mice During Embryo Implantation

MUC1 is a major anti-implantation mucin abundantly expressed on the apical surface of luminal and glandular uterine epithelia in mice and humans [13, 16]. Loss of MUC1 from the implantation site is believed to be essential for the establishment of a successful trophoblast-uterine interaction in vitro [13], and MUC1 is downregulated at the time of embryo implantation in mice [16]. Unexpectedly, unlike cNOD, MUC1 mRNA measured 4.97 ± 0.3-fold higher in the uteri of dNOD at E4.5 (Fig. 4A, compare DE4.5 with NE4.5). The expression of uterine MUC1 protein was also significantly higher ($P < 0.001$) in the uteri of dNOD dams during the time of implantation, as quantified in Western blotting (Fig. 4B, compare lanes 1 and 4 and their corresponding bar graphs) and as demonstrated in histological sections (Fig. 4C, compare A1-A2 with E1-E2). Progression of normal pregnancy to E6.5 in cNOD mice corresponded with an increase in MUC1 mRNA expression by 1.9 ± 0.2-fold (Fig. 4A, compare NE6.5 with NE4.5). Unpredictably, the uteri of pregnant, age-matched dNOD dams expressed significantly low levels ($P < 0.001$) of MUC1 mRNA (2.06 ± 0.17-fold less) (Fig. 4A, DE6.5 versus NE6.5) and MUC1 protein on E6.5 (Fig. 4B, compare lanes 2 and 4 and corresponding bar graphs). Alterations in the expression of MUC1 during peri- and postimplantation in the normally mated and ConA-induced decidualization in dNOD mice were also confirmed in histological sections (Fig. 4C, see B1-B2 and F1-F2). This aberrant pattern of MUC1 expression in early diabetic pregnancy was similarly observed in the uteri of pseudopregnant dNOD mice during E4.5 (DE4.5bid) and E6.5 (DE6.5bid) as determined by qPCR (Fig. 4A, DE4.5bid and DE6.5bid versus NE4.5bid and NE6.5bid), in WB (Fig. 4B, compare lanes 5 and 6 with lanes 7 and 8 and corresponding bar graphs) and in histological sections (Fig. 4C, compare C1and C2 and D1 and D2 with G1 and G2 and H1 and H2). The fold change in MUC1 mRNA measured 2.5 ± 0.17 higher ($P < 0.001$) and 2.1 ± 0.06 lower ($P < 0.001$) during DE4.5 bid and DE6.5 bid, respectively (Fig. 4A).

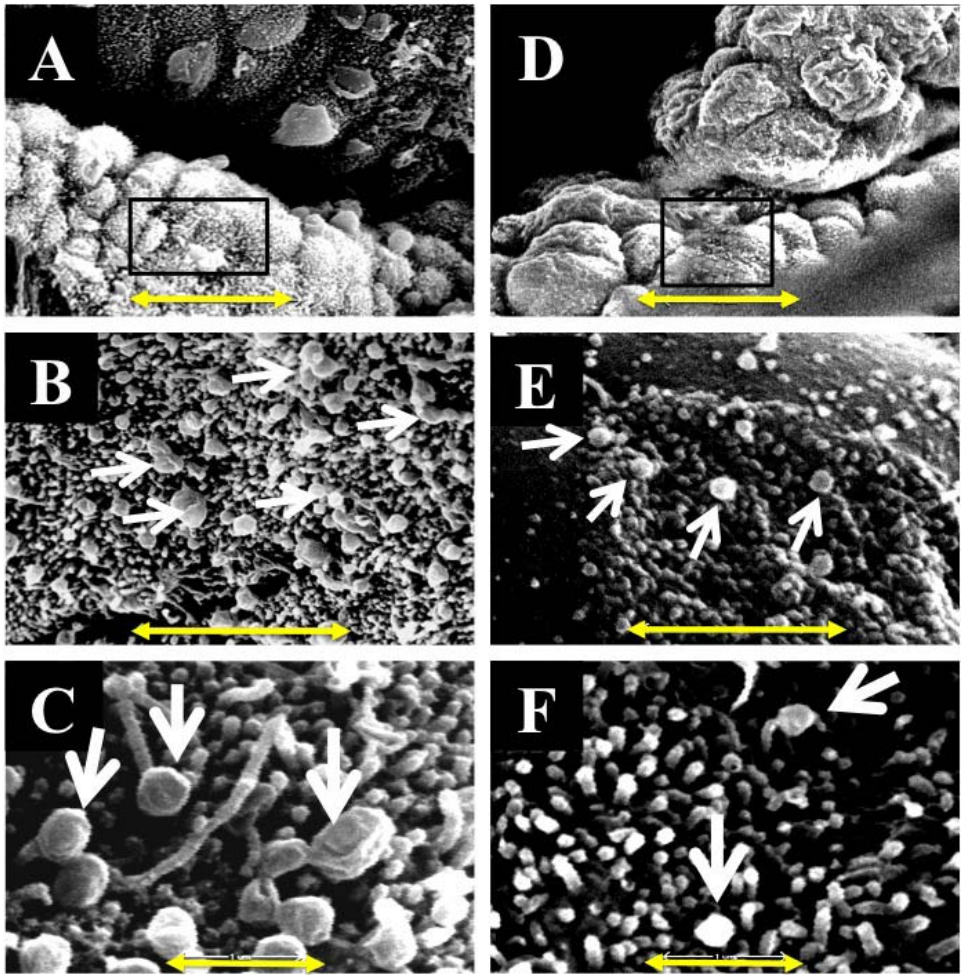

FIG. 2. Scanning electron microscopy features of cNOD (**A**–**C**) and dNOD (**D**–**F**) implantation sites on E4.5 showing prevalence of mature uterodomes (arrows). **B** and **C** and **E** and **F** compare at higher magnifications the typically observed differences in the population of mature uterodomes between implantation sites of cNOD (**A**) and dNOD (**D**), respectively. Bar = 10 μm (**A**, **D**), 2 μm (**B**, **E**), and 1 μm (**C**, **F**).

Uterine Expression of Phosphorylated STAT3 and NFκBp65 in dNOD Mice at the Peri- and Postimplantation Periods

Activated (phosphorylated) STAT3 and NFκB are two molecular biomarkers of uterine receptivity widely used to test for identification of the ''implantation window'' in mouse and in the human uterus [8, 9]. In view of our current findings of uterodome maturation failure in dNOD mice, we next examined uterine expression of STAT3 and NFκBp65 and their phosphorylated forms, pSTAT3-Ty705 and pNFκBp65, respectively, during embryo implantation. As shown in Figure 5A, unlike their expression in cNOD mice, the relative expression of pSTAT3-Ty705 was unexpectedly low in the uteri of dNOD mice at E4.5 but was induced at the postimplantation period at E6.5, respectively (Fig. 5A, compare lanes 1 and 2 with 3 and 4 and corresponding bar graphs). Of particular note is the failure of pSTAT3-Ty705 to mount during E6.5 in the ConA-induced decidualization in dNOD (Fig. 5A, compare lane 4 with 8 and their corresponding bar graphs). The latter may indicate some ''compensatory'' decidual response in STAT3 phosphorylation to delayed implantation in the normally mated dNOD mice. Similarly, the induction of pNFκBp65 was relatively less prominent in dNOD mice at E4.5 of their normal pregnancies and ConA-induced pseudopregnancy (Fig. 5B, compare lanes 3 and 7 and corresponding bar graphs). Interestingly, the pattern of pNFκBp65 expression paralleled that of pSTAT3-Ty705 in the uteri of dNOD mice during E4.5 and E6.5 of normal pregnancy (Fig. 5, A and B, compare lanes 3 and 4 and corresponding bar graphs). However, unlike STAT3, the phosphorylation pattern of NFκBp65 during E4.5bid and E6.5bid in dNOD mice was similar to that observed in the normally mated dNOD mice at E4.5 and E6.5, respectively (Fig. 5B, compare lanes 3 and 4 with 7 and 8 and corresponding bar graphs). This apparent discrepancy in the latter finding of the expression of pSTAT3-Ty705 and pNFκBp65 in response to ConA-induced decidualization in dNOD mice may be due to differences in underlying molecular mechanisms involved in the activation of the these two transcriptional factors in the artificially decidualized mouse endometrium. Nevertheless, the peculiarity in the temporal expression and phosphorylation of STAT3 and NFκBp65 in the context of delayed expression of these two activated proteins at 48 h past the time anticipated for embryo implantation in the normally mated dNOD mice may suggest delayed implantation response in these mice.

Uterine IFNγ Expression During Peri- and Postimplantation in dNOD Mice

The aberrant expression of IFNγ is pivotal in the development of diabetes and is an autoimmune-mediated

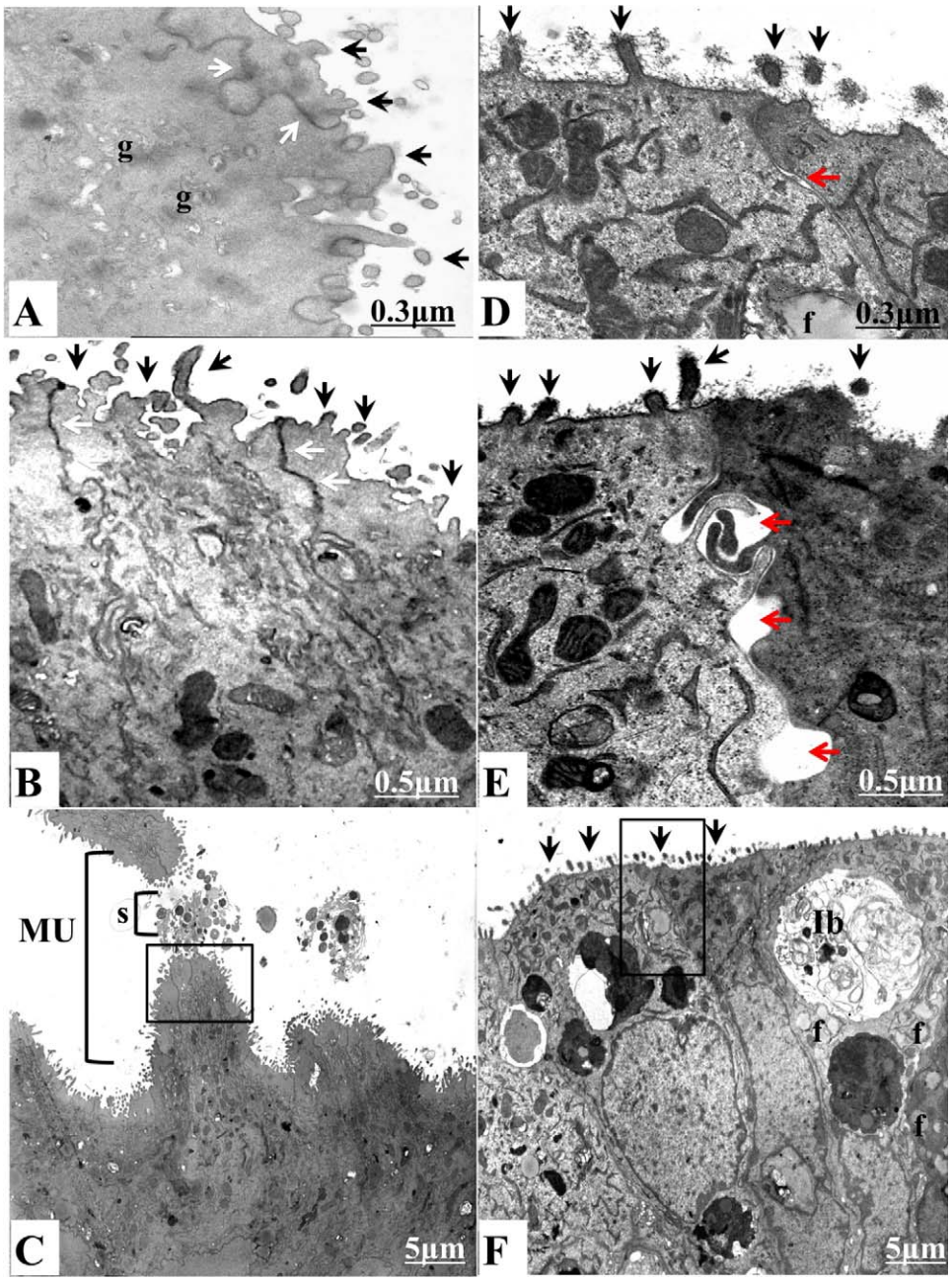

FIG. 3. TEM comparing ultrastructural features of cNOD (**A**–**C**) and dNOD (**D**–**F**) implantation sites on E4.5. **A** and **B** and **D** and **E** compare at higher magnification the apical surface of a mature uterodome bearing a relatively glycocalyx-free plasma membrane (**A** and **B**, black arrows) in cNOD mice versus a considerably thick glycocalyx-bearing apical plasma membrane projections in dNOD mice (**D**–**F**, black arrows). The formation of intercellular clefts between lateral plasma membranes of adjacent cells (**D** and **E**, red arrows), the disruption of lateral junctional complexes (compare between **D** and **E**, red arrows and **A** and **B**, white arrows) and the frequent presence of inclusion bodies (Ib; **F**) were the hallmarks of implantation sites uterodomes in dNOD dams on E4.5. MU, mature uterodomes; g, Golgi complex; f, lipid droplets; s, secretory materials. Bars = 0.3 μm (**A**, **D**), 0.5 μm (**B**, **E**), and 5 μm (**C**, **F**).

phenomenon in NOD mice [30, 31]. Importantly, IFNγ is critically involved in antagonizing the functions of nuclear PR signaling and in restricting the morphological transformation of uterine stromal cells during decidualization [22]. Based on the findings from the aforementioned studies and following our observation of implantation and decidualization defects in the uteri of dNOD mice, we examined the expression of IFNγ both at the mRNA level and in histological sections of uteri obtained from cNOD and dNOD mice during embryo implantation. Relatively high levels of IFNγ mRNA transcripts were detected in the uteri of pregnant and pseudopregnant dNOD mice relative to those of cNOD mice at E4.5 and E6.5 (Fig. 6A, compare lanes 1 and 2 with 3 and 4). Contrary to the previously reported normal pattern of IFNγ detection in normoglycemic mice [32] in which positive immunolabeling was detected in what is believed to be uterine natural killer (uNK) cells in the stroma proximal to decidual sinuses (Fig. 6B, see A–H), an intense immunoreaction was found to be associated with the epithelial (luminal and glandular) and stromal cells in uteri of normally mated and ConA-induced pseudopregnant dNOD mice (Fig. 6B, see I–P).

Uterine PR and PIASy Expression and Their Colocalization in cNOD and dNOD Mice at Peri- and Postimplantation

Uterine nuclear PR A and PR B are key modulators of uterine inflammatory signals during decidualization and are critically involved in regulating MUC1 expression [20]. The mouse uterus is a PR A-dominated endometrium, and changes to the expression of both PR isoforms A and B reflect a parallel fluctuation in serum progesterone levels in this rodent species [33]. Significantly elevated levels of serum progesterone ($P < 0.01$) were measured in the blood of dNOD mice during E4.5 (see Supplemental Fig. S5). The expression of PIASy is a known modifier of nuclear PR signaling in human and murine uterine cells, including those mediating decidualization and MUC1 expression in vitro [21, 22]. Therefore, in view of our findings of poor uterine decidualization and aberrant expression of MUC1 in the uteri of normally mated and pseudopregnant dNOD mice, we examined the protein expression of PR and PIASy and their immunohistochemical colocalization in the uteri of cNOD and dNOD mice during peri- and postimplantation.

PR expression in the uteri of cNOD and dNOD mice at peri- and postimplantation. During implantation in cNOD mice at E4.5, the expression levels of both nuclear isoforms of PR and especially that of PR B were significantly reduced ($P < 0.001$) to nearly undetectable levels (Fig. 7A, compare lanes 1 and 2 and corresponding bar graphs). However, the uterine expression of both progesterone receptor isoforms was upregulated after successful embryo implantation in the normally mated cNOD mice at E6.5 (Fig. 7A, compare lanes 1 and 2 and corresponding bar graphs). Unexpectedly, uteri of dNOD mice were found to express higher-than-normal levels of PR A but not PR B at E4.5 (Fig. 7A, compare lanes 3 and 1 and corresponding bar graphs), whereas reduced expression of both receptor isoforms was observed in all dNOD mice examined at E6.5 (Fig. 7A, compare lanes 3 and 4 with 1 and 2 and corresponding bar graphs). Importantly, uterine PR B expression was undetectable during the induction of artificial decidualization with ConA beads in both cNOD and dNOD mice, respectively. However, expression of PR A but not PR B was aberrantly induced in the uteri of dNOD mice on pseudopregnancy E4.5 rather than on E6.5 (Fig. 7A, compare lanes 7 and 8 and corresponding bar graphs).

PIASy expression and its colocalization with nuclear PR in uteri of cNOD and dNOD mice at peri- and postimplantation. During the progression of pregnancy in cNOD mice, decidual PIASy protein showed a steady increase in its production, with the largest amount detected on E6.5 of pregnancy (Fig. 7B, see lanes 1 and 2 and corresponding bar graphs). Immunohistochemical labeling revealed an intense immunostaining of PIASy in both stromal and epithelial compartments on E6.5 of normal pregnancy (Fig. 8, compare B1 with B2). However, colocalization of PIASy with PR was markedly evident at E4.5 rather than at E6.5 in the uterine epithelial cells of normally mated cNOD mice (Fig. 8, compare C1 and D1 with C2 and D2 and corresponding bar graphs). Unexpectedly, during the induction of deciduoma in cNOD on E4.5bid, rather than on E6.5bid, PIASy protein expression was induced (Fig. 7B, compare lanes 1 and 2 with 5 and 6 and corresponding bars graphs; Fig. 8, compare B3 and B4 and corresponding bar graphs). Nevertheless, PIASy colocalization with PR sites was more evident in the uterine epithelium at E6.5bid than E4.5bid in the cNOD mice (Fig. 8, compare D3 and D4 and corresponding bar graphs). Thus, it appears that the presence of an implanted embryo might have influenced PIASy expression and promoted its recruitment to the PR binding sites in a normally decidualized uterus in cNOD mice.

Overly diabetic dNOD mice showed a very different PIASy expression pattern and its colocalization with PR than those of pregnant and pseudopregnant cNOD mice. Decidual PIASy expression was undermined in the uteri of dNOD mice at E6.5 and E4.5bid as revealed by WB (Fig. 7 B, see lanes 3 and 4 and 7 and 8 and corresponding bar graphs). Surprisingly, and despite apparent discrepancy in the expression pattern of PIASy during the aforementioned gestational days in dNOD mice, semiquantitative analysis of immunostaining intensity demonstrated an increased colocalization of the two proteins in the epithelial and stromal compartments of poorly decidualized uteri in dNOD mice at E6.5 and E6.5bid rather than on E4.5 and E4.5bid, respectively (Fig. 8, compare D6 and D8 with D5 and D7 and corresponding bar graphs). It is likely that abnormally high levels of IFNγ might have driven the aberrant expression of PIASy and its colocalization with nuclear PR in dNOD mice during implantation. However, the lack of a possible inhibitory role for the attenuated phosphorylation of NFκBp65 to the uterine expression of PIASy and its (PIASy) tendency to colocalize to PR sites in the dNOD mice at implantation cannot be ruled out at present. Based on the finding obtained in the present study, the molecular events involving a possible role for IFNγ in the association with morphological features of implantation defects in dNOD mice are being proposed as illustrated in Figure 9.

DISCUSSION

The present study examined morphological and molecular features of endometrial receptivity in dNOD mice. High rates of mid-gestational fetal resorption and poor pregnancy outcomes in dNOD mice have suggested that this mouse strain may be a model of intrauterine growth restriction, and these outcomes are thought to be mediated, at least in part, by an abnormally high level of IFNγ production in the uteri of dNOD mice during gestation [3]. Of particular note is the current finding of an inability of dNOD mice, which express high levels of IFNγ in their uteri, to generate a receptive uterine milieu at the time anticipated for implantation to occur. This

FIG. 4. Detection of MUC1 expression in uteri of normally mated and ConA-induced pseudopregnant cNOD and dNOD mice during peri- and postimplantation by qPCR (**A**), in WB (**B**) and in histological sections (**C**), respectively. Data are mean fold changes in MUC1 mRNA in **A**; columns in **B** represent mean ± SEM values of MUC1/GAPDH chemiluminescence for all lanes within the respective WB, revealing an aberrant overexpression of MUC1 in uteri of normally mated and ConA-induced pesudopregnant dNOD mice on E4.5 and E4.5bid, respectively. Time course immunofluorescence detection of MUC1 in mid-sagittal sections of implantation sites of cNOD and dNOD mice during peri and postimplantation in **C** revealed high intensity of MUC1 immunolabeling in the uterine epithelium of dNOD mice on E4.5 (**C**, **E1**–**E2** versus **A1**–**A2**) and E4.5bid (**C**, **G1**–**G2** versus **C1**–**C2**), respectively. Unexpectedly, unlike the cNOD mice, uterine MUC expression was greatly reduced ($P < 0.001$) in dNOD mice on E6.5 and E6.5bid at the mRNA level (**A,** compare NE6.5 and NE6.5bid with DE6.5 and DE6.5bid), in WB (**B**, compare lanes 2 and 4 with lanes 6 and 8 and corresponding bar graph), and in histological sections (**C**, compare **B1**–**B2** and **D1**–**D2** with **F1**–**F2** and **H1**–**H2**). Data in **A**, **B** and **C** are a representation of one out of three independent experiments with similar results. n = 3–5 in all groups per experiment, and different letters on the bar graphs in **A** and **B** are significantly different at 95% confidence. Bar = 100 μm.

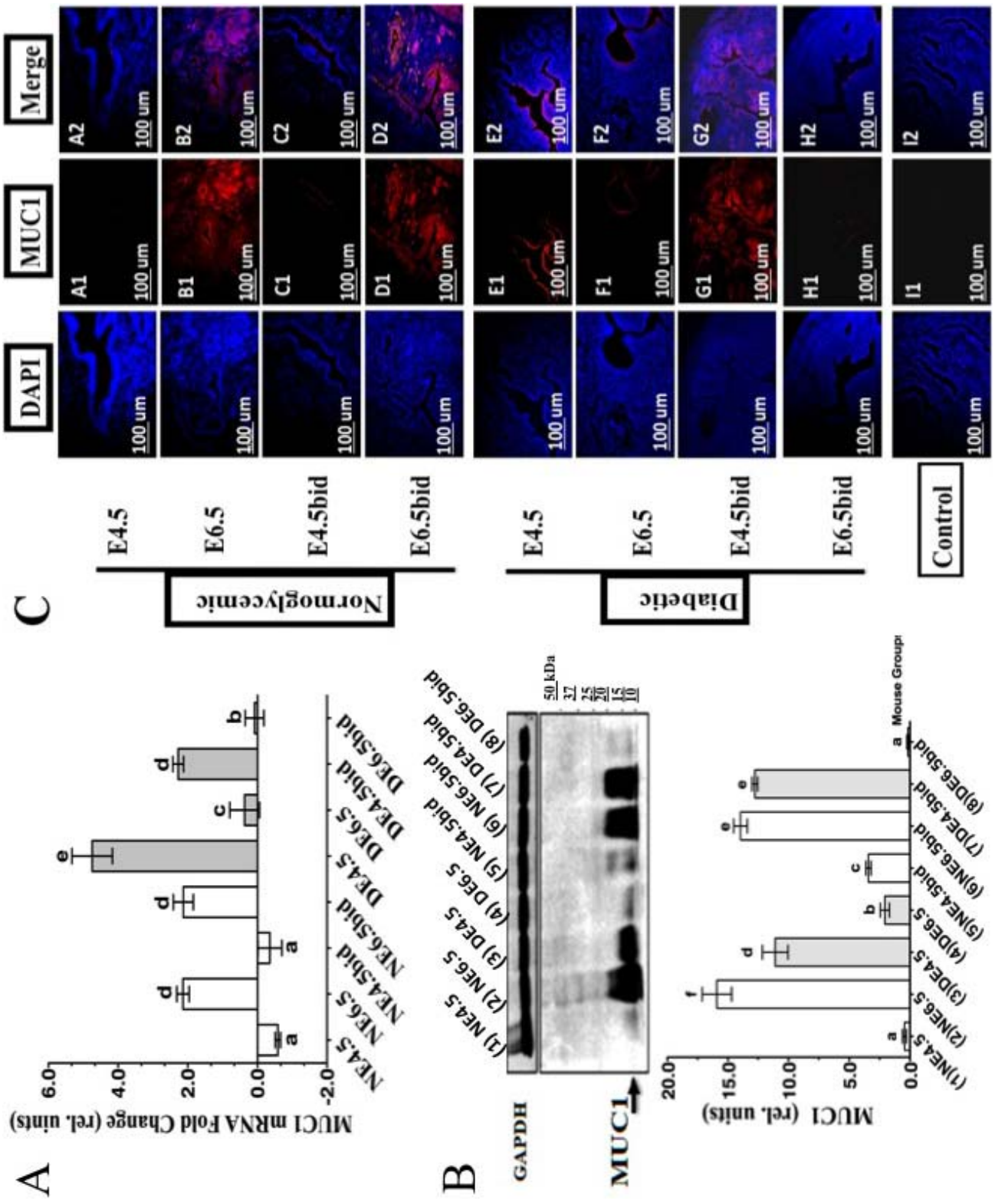

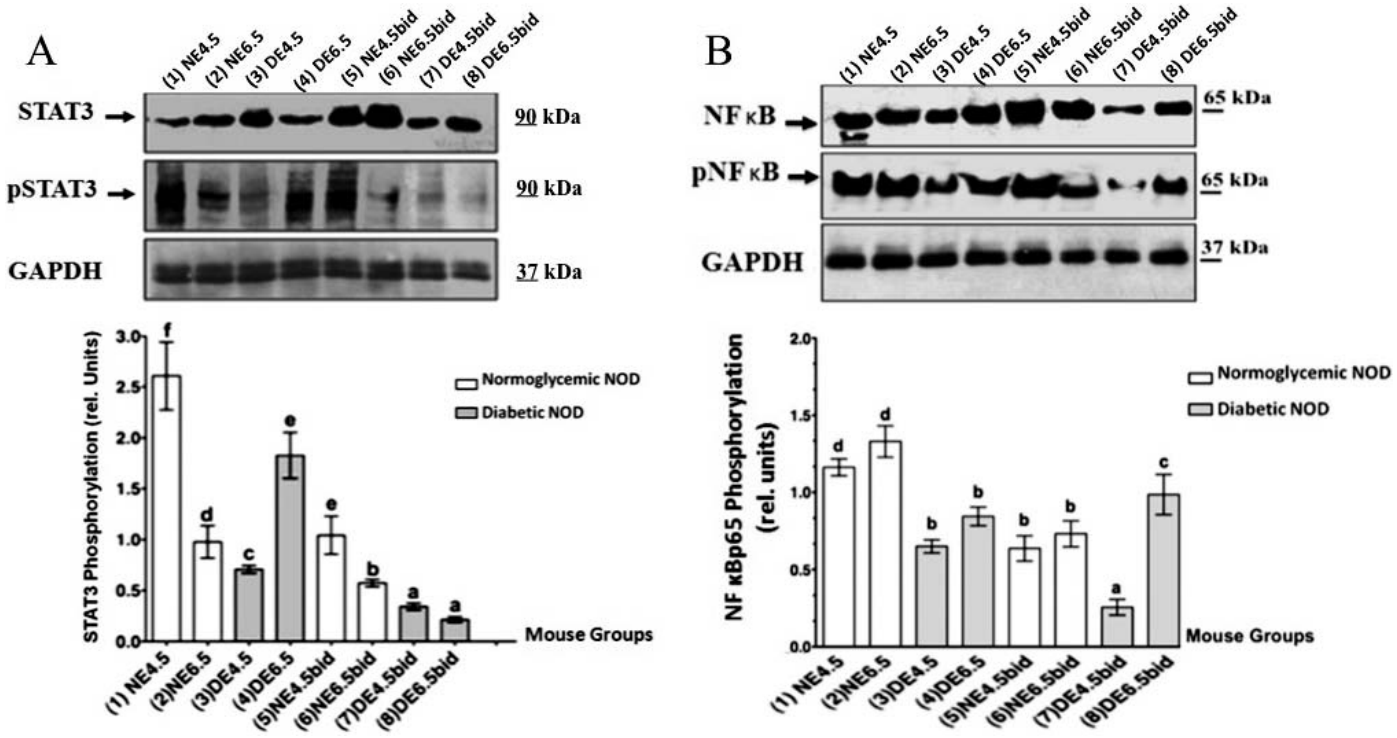

FIG. 5. WB detection of STAT3 (**A**) and NFκBp65 (**B**) and their phosphorylated forms pSTAT3-Ty705 and pNFκBp65 in the uteri of normally mated and ConA-pseudopregnant dNOD and cNOD mice during peri and postimplantation, respectively. **A**) Data show reduced expression ($P < 0.01$) of nuclear pSTAT3-Ty705 on E4.5 and E4.5bid in dNOD (compare lanes 1, 3, 5 and 7 and corresponding bar graphs). Induction of pSTAT3-Ty705 expression on E6.5 in dNOD (**A**, lane 4 and representative bar graphs) is likely a manifestation of delayed implantation, whereas failure of STAT3-Ty705 phosphorylation on E4.5bid and E6.5bid, respectively (lane 7 and 8 and corresponding bar graphs), may indicate inability of dNOD mice to sustain artificial decidualization. **B**) Expression of nuclear pNFκBp65 is significantly low ($P < 0.01$) in the uteri of normally mated dNOD mice on E4.5 and E6.5, respectively (compare lanes 3–4 and 7–8 with lanes 1–2 and 5–6 and corresponding bar graphs). Values in the bar graphs represent the mean ± SEM of results obtained in three sets of experiments with similar outcome. Different letters on the bar graphs in **A** and **B** are significantly different at 95% confidence. n = 3–5 in all groups per experiment.

observation was manifested in high rates of peri- and postimplantation failure, defective maturation of uterodomes; lack of timely phosphorylation of STAT3 and NFκBp65 and the abnormal induction of uterine MUC1 and PIASy expression.

Several possible explanations exist for the high percentage of peri-implantation loss in the uteri of dNOD mice reported in the present study. Although it is likely that IFNγ-mediated embryotoxicity may have been predisposed to restricted peri-implantation embryo development, a possible role for maternal hyperglycemia in inflicting the high rate of embryo demise cannot be ruled out. dNOD mice were persistently hyperglycemic throughout their gestation (Supplemental Fig. S1). The contribution of murine hyperglycemia to pregnancy failure in diabetes has been studied both in vitro and in vivo. In an in vitro model of murine peri-implantation under conditions mimicking poorly controlled maternal diabetes, Fraser et al. [34] identified certain hyperglycemia-induced developmental delays during the precompaction morula stage that contributed to failed postimplantation embryo development observed in diabetic mice. In IFNγ-deficient dNOD mice, Seaward et al. [35] noted that failed postimplantation pregnancy is likely a hyperglycemia-mediated event. However, an etiological role for IFNγ-mediated embryolethality in restricting postimplantation embryo development in dNOD mice expressing IFNγ could not be excluded [3, 35]. In pregnant, overly diabetic dNOD mice, Burke et al. [3] attributed reduction in fetal trophoblastic areas of the placenta and morphological features of embryonic intrauterine growth restriction and placental insufficiency to pathologically high levels of IFNγ [3]. Indeed, high-level production of IFNγ at implantation sites is disadvantageous to peri-implantation gestational success [36]. Glynn et al. [37] reported a detrimental role for high levels of IFNγ on transforming growth factor beta-1 (TGFb1)-induced maternal tolerance during early pregnancy, and they suggested a causative role for aberrant expression of this pleotrophic, proinflammatory cytokine in pregnancy failure in women with recurrent miscarriages [37]. Embryotoxicity mediated by IFNγ has also been demonstrated in vitro in mouse trophoblast maturation assays [38, 39]. Fontana et al. [38] found that exogenous administration of IFNγ drastically inhibited growth of the inner cell mass, impairing the outgrowing stage and resulting in the degeneration of trophoblast cells in a manner similar to changes occurring in embryos exposed to sera from women suffering from recurrent spontaneous abortions [39]. It has also been shown that IFNγ-mediated embryolethality involves the cell surface expression of class I major histocompatibility complexes (MHC) in human and murine trophoblast cells [40]. Trophoblast cells in humans and rodents do not normally express such cell surface determinants, which are involved in MHC-class1-restricted maternal cytotoxic T-cell recognition and removal [40]. In an unpublished observation of the uteri of dNOD mice on E4.5 and E6.5, we noticed that implantation sites and embryonic cellular remnants were heavily infiltrated with CD45-positive cells, which is suggestive of an increased T-cell recognition of embryonic components very early on in the pregnancies of dNOD mice. Therefore, it is tempting to speculate that late onset

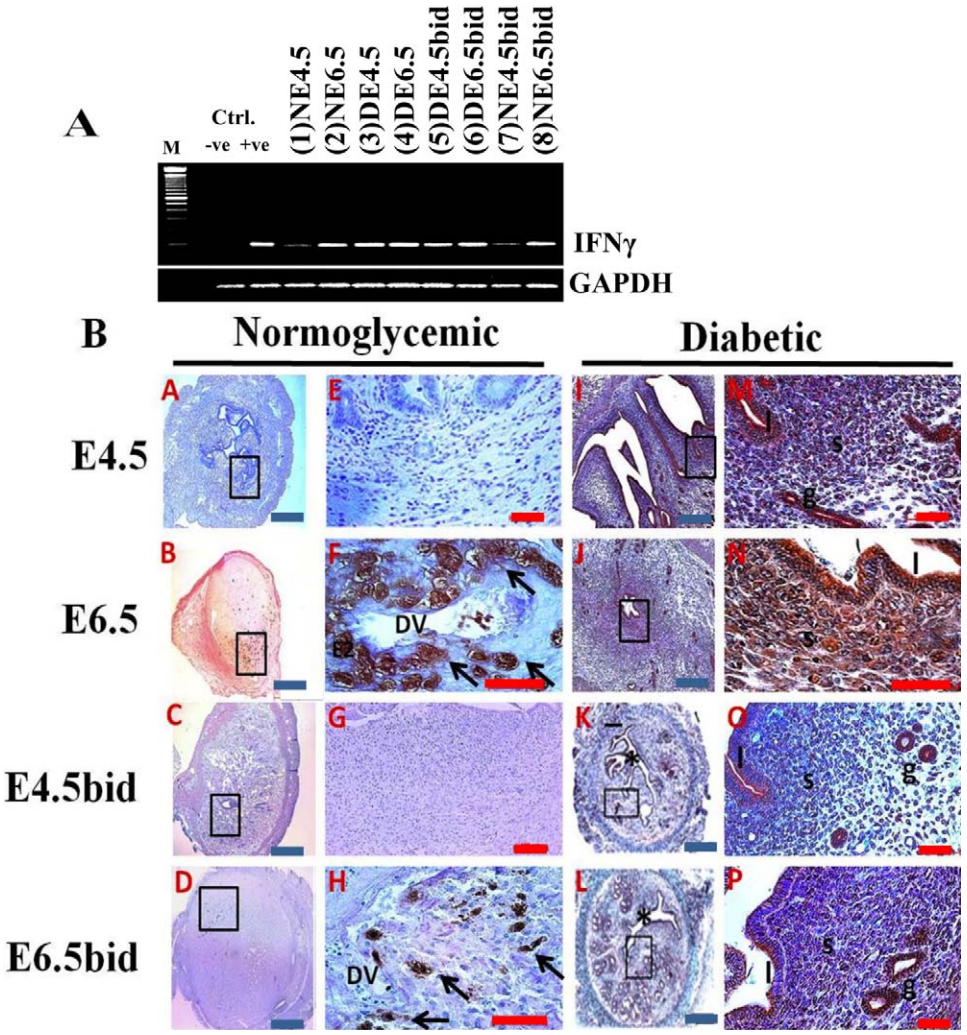

FIG. 6. Detection of changes in uterine IFNγ gene expression by semiquantitative PCR (**A**) and in histological sections (**B**) in the normally mated and ConA-induced pseudopregnant cNOD and dNOD mice during peri and postimplantation. **A**) IFNγ mRNA was expressed in high levels in the uteri of dNOD mice throughout early pregnancy and/or pseudopregnancy days 4.5 and 6.5, respectively (**A**, compare lanes 3–6 with lanes 1–2 and 7–8, respectively). Transcripts from lipopolysaccharides-stimulated mouse peritoneal cells tested for INFγ mRNA were loaded to the positive (+ve) control lane, and IFNγ complementary sense sequence "gtctggcctgctgttaaagc" was added to the PCR reaction to generate a negative (-ve) control. **B**) Time-course IHC detection of uterine IFNγ in histological sections of cNOD (**A**–**H**) and dNOD (**I**–**P**) mice at the peri- and postimplantation, and in the ConA-induced pseudopregnancy. **E**–**H** and **M**–**P** show at higher magnifications of the corresponding inset images in **A**–**D** and **I**–**L**, respectively, featuring IFNγ immunolocalization in uNK cells on E6.5 (**F**, arrows) and E6.5bid (**H**, arrows). A diffuse epithelial and stromal immunolabeling was detected in the uteri of dNOD mice on E4.5, E6.5, E4.5bid and E6.5bid (**M**–**P**), respectively; n = 3 mice per group per 3 sets of independent PCR experiments with similar outcome. DV, decidual vessels; * indicates uterine lumen; l, luminal epithelium; s, stroma; g, metrial glands. Blue bar = 100 μm; red bar = 50 μm

implantation response in the uteri of dNOD mice is exposing the conceptus to an increasing risk of prolonged and sustained exposure to a local cytotoxic milieu, thereby resulting in the high rate of failed implantation and postimplantation resorption in dNOD mice at E4.5 and E6.5, respectively. Indeed, using a cytokine multiplexing assay, we also confirmed the expression of an aberrant, IFNγ-inducing proinflammatory cytokine milieu in the uteri of dNOD mice at E6.5 represented by the upregulated expression of IL16, IL12p70, and IL27 (A.J.H. Albaghdadi and F.W.K. Kan, unpublished results). IL12 and IL27 are believed to induce a Th-1-committed immune response through a variety of mechanisms, some of which involve activation of pSTAT3-Ty705 in mammalian cells in vitro [41]. Furthermore, consistent with the currently reported delayed implantation and high rate of postimplantation resorption among dNOD mice, we have detected an anomalous expression ratio for IL1α:IL1β and that of IL1ra expression in the uteri of dNOD mice at E4.5 and E6.5, respectively (A.J.H. Albaghdadi and F.W.K. Kan, unpublished results). Besides its role in inducing phosphorylation of NFκB [42], IL1β has also been proposed to play a critical role in potentiating immunotolerance at the maternal-trophoectodermal interface, both at and beyond the WOI in viviparous animals [43]. IFNγ is potentially capable of downregulating IL1β through a variety of intracellular signaling pathways, some of which involve PIAS and/or suppressor of cytokine signaling (SOCS)-related mechanisms [44], and when administered exogenously, non-physiological concentrations of IFNγ inhibited the expression of IL1β in the rat uterus during implantation [45]. Furthermore, the loss of temporal regulation of the uterine expression of PR A and PR B during WOI and at the immediate postimplantation period in the uteri of dNOD mice is likely augmenting an IFNγ-related inhibition of the uterine/decidual expression of IL1β, NFκB, and LIF during murine implantation. Stimulation of uterine IL1β, NFκB, and LIF axis during WOI is critical to establishing pregnancy in the mouse and is linked to a

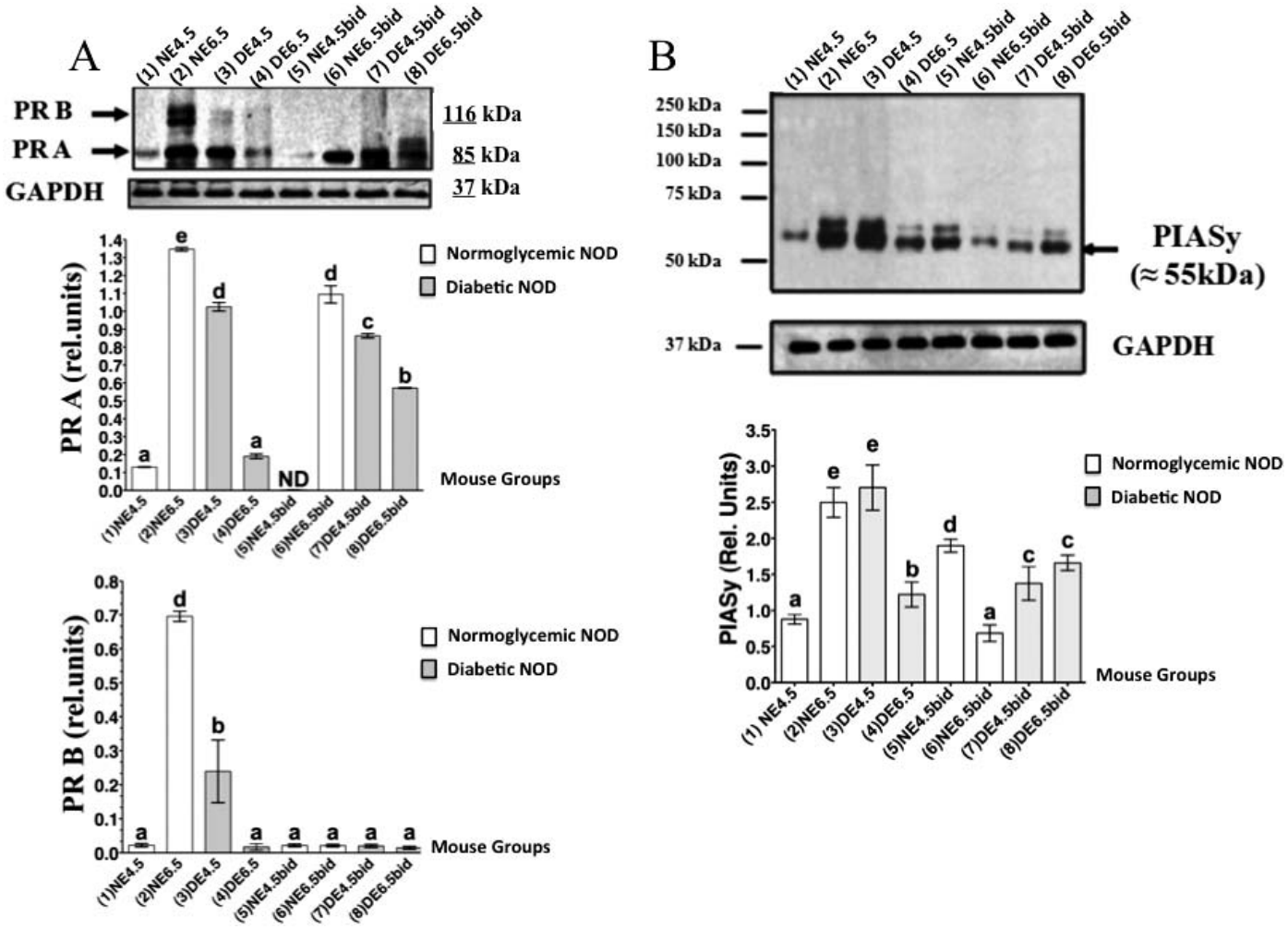

FIG. 7. WB detection of PR and PIASy in the uteri of cNOD and dNOD mice during implantation. Data in **A** reveal an aberrant expression of PR A during embryo implantation and in the ConA-induced decidualization in dNOD mice (compare lanes 3–4 and 7–8 with the remaining lanes and their corresponding bar graphs). The expression of PR B is likely embryo-dependent and its unusually reduced expression in the dNOD mice is likely reflecting poor endometrial response to embryo implantation. **B**) Representative WB detection of uterine PIASy during peri- and postimplantation in cNOD and dNOD indicating dependency of PIASy expression upon successful implantation and decidualization in the normally mated cNOD mice (compare lanes 1 and 2 with lanes 7 and 8 and corresponding bar graphs). The anomalous expression of uterine PIASy reciprocated implantation and decidualization failure in dNOD mice (see lanes 3 and 4, and lanes 7 and 8 and corresponding bar graphs). The bars in graphs **A** and **B** represent GAPDH averaged mean of PR (**A**) or PIASy (**B**) chemiluminescence ± SEM. Data shown in **A** and **B** represent results obtained in three independent experiments with similar outcome. n = 3–5 in all groups per experiment, and different letters on the bar graphs in **A** and **B** are significantly different at 95% confidence.

subsequent activation of a variety of downstream uterine mechanisms involved in regulating embryo-uterine interactions at implantation, such as certain Th-2-committed cytokines/chemokines and growth factors, namely IL6, IL8, GCSF, and GMCSF; cell adhesion molecules such as selectins, integrins, and heparin-binding EGF (HB-EGF) receptors; and enzymes and modulators of tissue remodeling such as metallopeptidases (MMPs) and their inhibitors (TIMPs), prostaglandin-endoperoxide synthase 2 (PTGS2) and aquaporins [46]. Thus, it appears that an intriguing, albeit complex, network of IFNγ-related molecular events including but not limited to dysregulated activation of the nuclear transcriptional factors pSTAT3-Ty705, pNFκBp65 and PR A, and the aberrant expression of some key Th-1 regulatory cytokines, namely IL1, IL12, and IL27 in the uteri of dNOD at E4.5 and E6.5 are jeopardizing the murine implantation cascade and are detrimental to peri- and post-implantation embryo development in diabetes.

Restricted maturation of uterodomes in the uteri of dNOD mice is mostly multifactorial in nature, possibly reflecting a combined action of high levels of progesterone secretion and profuse production of IFNγ in dNOD mice. Experimental evidence in rodents has established the necessity of the transformation of a microvillous apical plasma membrane into a smooth, flattened, albeit bulging plasma membrane at the site of uterodome formation for successful blastocyst attachment [6, 47]. Multiple maternal hormonal, cytokine, and paracrine-regulated mechanisms were shown to be central to the latter uterine epithelial membranous transformation occurring at implantation in rodents [6, 47]. Among the latter maternal factors, progesterone is critical to endometrial receptivity [47]. Under nondiabetic conditions, physiologically normal levels of progesterone induced elongation but not widening of tight junctions, loss of adherens junctions, and downregulation of key desmosomal proteins, thereby reducing the complexity of the desmosomal structure of the lateral uterine plasma membrane during implantation in mice [47]. It is presently unclear whether the abundantly high level of serum progesterone compiled with that of a locally overexpressed MUC1 may have inflicted the currently observed dysmorphism in the lateral plasma membrane, including widening of the junctional

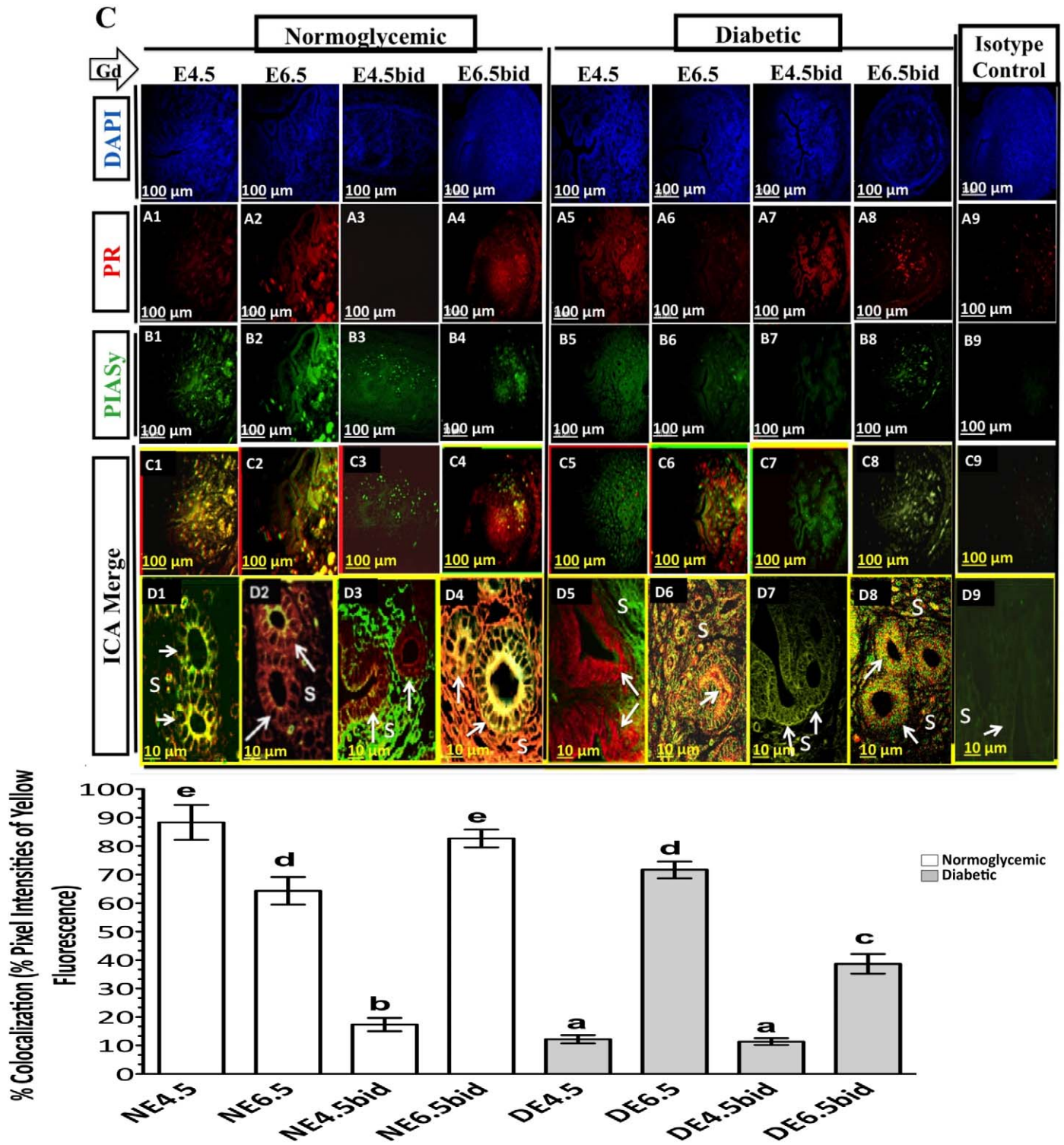

FIG. 8. Representative time-course fluorescent immunohistochemistry staining of the uterus for PR (red) (**A1**–**A8**), and PIASy (green) (**B1**–**B8**) in the normally mated and in ConA-pseudopregnant cNOD and dNOD mice, respectively. Photomicrographs in **D1**–**D8** show at higher magnifications of **C1**–**C8** the typically observed differences in the pattern and intensity of colocalization of PIASy with nuclear PR in the epithelial (arrows) and stromal (S) compartments between cNOD (**C1**–**C4** and **D1**–**D4** and corresponding bar graphs) and dNOD (**C5**–**C8** and **D5**–**D8** and corresponding bar graphs) during peri-implantation on E4.5 and E4.5bid, and postimplantation on E6.5 and E6.5bid, respectively. Absence of an embryo resulted in lack of an actual colocalization between PIASy and PRs in both cNOD and dNOD on E4.5bid (**D3** versus **D7** and corresponding bar graphs). Photomicrographs in **A9** and **B9** are representative isotype control stained uterine sections for PR and PIASy, respectively. Photomicrographs C9 and D9 are representative intensity correlation analysis merge images of A9 and B9 correspondingly. n = 3 per group in each of 3 sets of experiments with similar outcome. Different letters on the bar graphs are significantly different at 95% confidence. Bar = 100 µm (**A1**–**A9**, **B1**–**B9**, **C1**–**C9**), 10 µm (**D1**–**D9**).

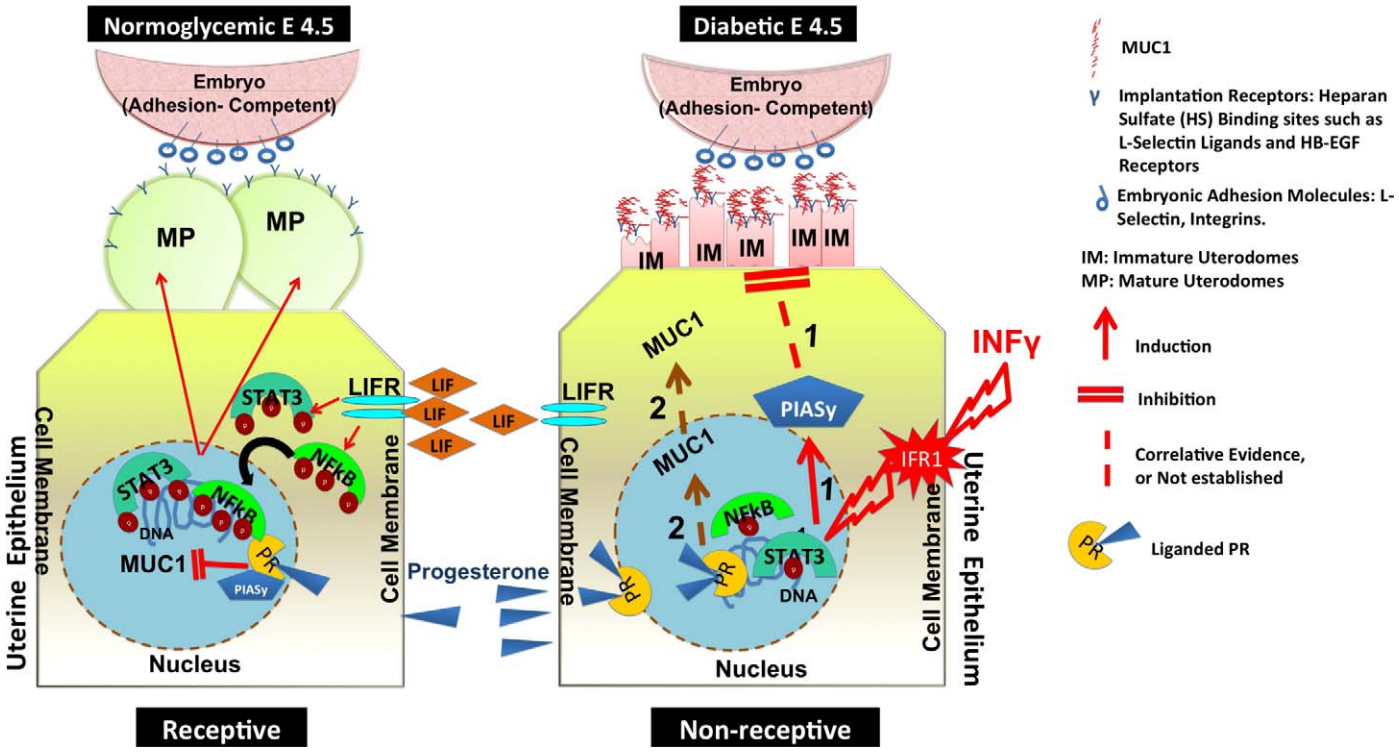

FIG. 9. Schematic representation of proposed molecular events associated with morphological features of implantation failure in the dNOD mice. During the receptive phase in normoglycemic mice (diagram to the left), LIF, acting through its cell surface receptor (LIFR) mediates phosphorylation and nuclear translocation of the transcription factors STAT3 and NFκBp65 and subsequently inducing maturation of uterine pinopodes. The illustration on the right depicts the IFNγ-mediated intracellular events linked to uterodome maturation failure during embryo implantation in dNOD mice. Acting through its cell surface receptor (IFR1), IFNγ is likely initiating a series of transcriptional events which are incompatible with maturation of uterodomes, such as induction of PIASy expression, reduced nuclear expression of phosphorylated STAT3 and NFκBp65 and reduced bioavailability of LIF as illustrated in pathway 1. Pathway 2 speculates on a possible, in vivo PR-mediated induction of MUC1 expression in the uterine epithelium of dNOD mice at implantation.

complexes in dNOD mice at the time of embryo implantation. Overexpressed MUC1 weakens the integrity of junctional complexes in the lateral plasma membrane in an E-cadherin and beta-catenin-dependent mechanism [48]. Therefore, it is likely that a defect(s) in the mechanism(s) regulating uterine MUC1, allowing its overexpression on day 4.5 of pregnancy in dNOD mice, may have predisposed to uterodome maturation failure, in part through altering their apical and lateral uterine epithelial plasma membranes to incur nonreceptivity. Nevertheless, a possible role for the attenuated uterine production of LIF and the abnormally high local levels of IFNγ in inducing the aforementioned malformations in the apical and lateral plasma membranes of uterine epithelium cannot be excluded. At pathologically high concentrations, IFNγ is capable of inducing endocytosis of tight junctional proteins, thereby inducing vaculorization of apical and lateral plasma membranes in mammalian epithelial cells in vitro [49]. Moreover, IFNγ inhibits LIF-mediated secretory activity involved in the maturation process of uterine pinopodes [50], and IFNγ has also been described as a potent inhibitor of growth factors such as platelet-derived growth factor, transforming growth factor-beta, and the cytokines TNFα and IL1-induced LIF as demonstrated in human endometrial cells in vitro [11]. In mouse and human uteri, LIF acts in conjunction with biological mediators released by the blastocysts to induce maturation of the apical uterodomes through phosphorylation and activation of STAT3 and NFκBp65 signaling during the WOI [8, 10, 51]. Although the exact mechanism of IFNγ-mediated LIF inhibition in uterine cells is not well understood, a suggested role for PIASy-mediated inhibition of LIF signaling seems likely. Nelson et al. [52] showed that in yeast two-hybrid assays and in mammalian cells in vitro, PIASy interferes with DNA binding of the nuclear transcriptional factor p53 and blocks its expression of downstream target genes. It is recognized that p53 signaling is indispensible for the establishment and progression of early pregnancy [53], and LIF is a known p53 downstream-response cytokine gene [53]. In view of our current findings of the aberrant induction of PIASy, inhibition of STAT3 phosphorylation and defective uterodome maturation during the time expected for the embryo to implant in dNOD mice, further studies are warranted to elucidate the nature of the interaction between PIASy and p53 at implantation under normal and diabetic conditions.

Among the features suggestive of restricted uterine receptivity in dNOD mice was the upregulation of uterine MUC1, both at the transcriptional and translational levels, at the time of implantation. Despite reported differences in molecular mechanisms involved in the regulation of MUC1 expression at implantation in mice and humans [13, 16], it is largely held that the downregulation of MUC1 expression during the implantation window in the mouse is largely maternally regulated through hormones and their downstream effecter molecules such as cytokines and chemokines [16, 20, 21]. Among the cytokines involved in regulation of murine and human MUC1 expression is PIASy [21]. PIASy is a downstream IFNγ response protein involved in damping IFNγ-induced cellular responses and in antagonizing PR-mediated transcription in the mouse and human uterus [22]. Brayman et al. [21] reported a potent, dose-dependent inhibitory effect of PIASy on both basal and progesterone-stimulated MUC1 expression in mouse and

human uterine cells in vitro [21]. It is believed that PIASy-mediated MUC1 inhibition resulted from the recruitment of nuclear corepressors to the PR-response element of the MUC1 promoter in response to PIASy colocalization to nuclear PR [21]. It is also believed that colocalization of PIASy to liganded-PR inhibits IFNγ signaling in a regulatory feedback mechanism that recruits certain nuclear corepressors of transcription such as C-terminal binding proteins and receptor-interacting protein 140, thereby providing resistance against IFNγ-mediated cytotoxicity during progression of early pregnancy for the decidualizing cells [21, 22]. Despite the inhibitory role of high levels of IFNγ on P4-mediated transcription, at least in part by promoting the formation of a PIASy-PR complex and by recruiting different nuclear corepressors of PR in the decidualizing mouse uterine stromal cells [22], little is known about the role of PIASy in modulating mouse uterine epithelial and stromal responses including MUC1 expression and the induction of decidualization during implantation in diabetic subjects. Based on the rationale that MUC1 expression in uterine cells is downregulated by the recruitment of PIASy to nuclear PR binding sites [21], we carried out a linear regression analysis to examine whether there is a correlation between uterine MUC1 mRNA expression during early pregnancy in normoglycemic and diabetic NOD mice and the degree of colocalization of PAISy and PRs in these uteri. Supporting the previously reported potent inhibitory effect of PIASy in the downregulation of MUC1 at the transcriptional level in vitro [21], our finding of a strong positive correlation between MUC1 expression and the extent of colocalization of PIASy to nuclear PR during early pregnancy in the uteri of normally mated cNOD and dNOD mice (see Supplemental Fig. S6) also suggests a similar role for PIASy in regulating uterine MUC1 transcription in vivo. Except for diabetic pseudopregnancy, linear regression analysis revealed a significant correlation between increased recruitment of PIASy to nuclear PR sites and the fold changes in MUC1 mRNA in normally mated cNOD and dNOD mice. The calculated repressive effect of PIASy recruitment to PR sites and MUC1 mRNA expression was significantly correlated at the 95% confidence level (see Supplemental Fig. S6, A–C). The failure to induce PR B expression impacted both the colocalization and correlation analyses in the diabetic pseudopregnant uteri (see Supplemental Fig. S6D) However, the exact contribution of PR B to the regulation of MUC1 expression in the artificially induced decidua in cNOD and dNOD mice remains unclear at present. It is possible that the inhibited expression of uterine PR B during early pseudopregnancy may have prevented colocalization of PIASy to nuclear PR in the uteri of both strains of mice. The latter finding is suggestive of the requirement for embryo-derived signals and the involvement of uterine PR B mediated responses in the modulation of PIASy expression in the normal mouse uterus during implantation.

In conclusion, the results obtained in the present study indicate that dNOD mice, in addition to being a proposed model of diabetes-related intrauterine growth restriction [3], can also be considered a model of delayed implantation and early pregnancy failure. Although the exact nature of interactions between the downstream signaling pathways of IFNγ and PR A and PR B in differentially regulating uterine PIASy and MUC1 expression in normal and diabetic mouse uteri during early pregnancy awaits further investigation, the present study provided an insight into molecular cues likely involved in the generation of a nonreceptive or hostile endometrium at the time of implantation in the diabetic subjects. Data obtained in the present investigation support a hypothesized pathological role for IFNγ and/or its downstream target PIASy in conferring endometrial resistance to implantation in diabetes. A possible mechanistic link to recurrent early pregnancy loss in the diabetic women may reside in the aberrant, IFNγ-associated dysregulation of molecular events critically involved in the generation of a receptive uterus during implantation in dNOD mice. The latter may include but is not limited to uterodome maturation failure and aberrations in MUC1 expression during implantation in diabetic subjects. Further translational studies may be necessary to determine whether restricted decidualization in the endometrium of diabetic women who are experiencing recurrent spontaneous abortion is mechanistically linked to a locally high IFNγ-induced resistance to progesterone signaling during embryo implantation. However, it may deem advantageous to assess benefits of suppressing IFNγ production relative to pregnancy outcome in diabetic and other IFNγ-mediated immune complicated pregnancies.

ACKNOWLEDGMENT

We thank Sandra J. Gendler from the Mayo Clinic (Arizona) for generously providing the anti-MUC1 CT2 antibody. We are also thankful for members of the community at Queen's University, Mr. Mathew Gordon and Mr. Jeffery Mewburn from the Imaging facility at the Cancer Research Institute, Mr. John Dacosta from the Department of Pathology and Molecular Medicine, and members of the Animal Care Services for their invaluable technical assistance. Our special thanks go to Xiaoghing Guo, for her assistance with designing primers for MUC1 and IFNγ.

REFERENCES

1. Platt MJ, Stanisstreet M, Casson IF, Howard CV, Walkinshaw S, Pennycook S, McKendrick O. St Vincent's declaration 10 years on: outcomes of diabetic pregnancies. Diabet Med 2002; 19:216–220.
2. Casson IF, Clarke CA, Howard CV, McKendrick O, Pennycook S, Pharoah PO, Platt MJ, Stanisstreet M, van Velszen D, Walkinshaw S. Outcomes of pregnancy in insulin dependent diabetic women: results of a five year population cohort study. BMJ 1997; 315:275–278.
3. Burke SD, Dong H, Hazan AD, Croy BA. Aberrant endometrial features of pregnancy in diabetic NOD mice. Diabetes 2007; 56:2919–2926.
4. Psychoyos A, Nikas G. Uterine pinopodes as markers of uterine receptivity. Assist Reprod Rev 1994; 4:26–32.
5. Murphy CR, Shaw TJ. Plasma membrane transformation: a common response of uterine epithelial cells during the peri-implantation period. Cell Biol Int 1994; 18:1115–1128.
6. Psychoyos A. Hormonal control of ovoimplantation. Vitam Horm 1973; 31:201–256.
7. Kaneko Y, Lindsay LA, Murphy CR. Focal adhesions disassemble during early pregnancy in rat uterine epithelial cells. Reprod Fertil Dev 2008; 20: 892–899.
8. Nakamura H, Kimura T, Ogita K, et al. NFκB activation at implantation window of the mouse uterus. Am J Reprod Immunol 2004; 51:16–21.
9. Teng CB, Diao HL, Ma XH, Xu LB, Yang ZM. Differential expression and activation of Stat3 during mouse embryo implantation and decidualization. Mol Reprod Dev 2004; 69:1–10.
10. Chen JR, Cheng J, Shatzer T, Sewell L, Hernandez L and Stewart CL. Leukemia inhibitory factor can substitute for nidatory estrogen and is essential to inducing a receptive uterus for implantation but is not essential for subsequent embryogenesis. Endocrinol 2000; 141:4365–4372.
11. Arici A, Engin O, Attar E, and Olive DL. Modulation of leukemia inhibitory factor gene expression and protein biosynthesis in human endometrium. J Clin Endocrinol Metab 1995; 80:1908–1915.
12. Raghupathy, R, Makhseed M, Azizieh F, Omu A, Gupta M and Farhat R. Cytokine production by maternal lymphocytes during normal human pregnancy and in unexplained recurrent spontaneous abortion. Hum Reprod 2000; 15:713–718.
13. Singh, H Nardo, L Kimber SJ, Aplin JD. Early stages of implantation as revealed by an in vitro model. Reproduction 2010; 139:905–914.
14. Gendler SJ, Spicer AP. Epithelial mucin genes. Annu Rev Physiol 1995; 57:607–634.
15. Brayman M, Thathiah A, Carson DD. MUC1: a multifunctional cell surface component of reproductive tissue epithelia. Reprod Biol Endocrinol 2004; 7; 2:4.
16. Surveyor GA, Gendler SJ, Pemberton L, Das SK, Chakraborty I, Julian J,

Pimental RA, Wegner CC, Dey SK, Carson DD. Expression and steroid hormonal control of Muc-1 in the mouse uterus. Endocrinol 1995; 136: 3639–3647.
17. Horne AW, Lalani EN, Margara RA, Ryder TA, Mobberley MA, White JO. The expression pattern of MUC1 glycoforms and other biomarkers of endometrial receptivity in fertile and infertile women. Mol Reprod Dev 2005; 72:216–229.
18. Robb L, Li R, Hartley L, Nandurkar HH, Koentgen F, Begley CG. Infertility in female mice lacking the receptor for interleukin 11 is due to a defective uterine response to implantation. Nature Med 1998; 4:303–308.
19. Palfi M, Jablonowska B, Matthiesen L. Circulating interferon-gamma- and interleukin-4-secreting cells in recurrent spontaneous abortions. Am J Reprod Immunol 1999; l 41:257–263.
20. Dharmaraj N, Wang P and Carson DD. Cytokine and progesterone receptor interplay in the regulation of MUC1 gene expression. Mol Endocrinol 2010; 24:2253–2266.
21. Brayman MJ, Dharmaraj N, Lagow E, Carson DD. MUC1 expression is repressed by protein inhibitor of activated signal transducer and activator of transcription-y. Mol Endocrinol 2007; 21:2725–2737.
22. Zoumpoulidou G, Jones MC, de Mattos SF, Francis JM, Fusi L, Lee YS, Christian M, Varshochi R, Lam EF, Brosens JJ. Convergence of interferon-γ and progesterone signaling pathways in human endometrium: role of PIASy (protein inhibitor of activated signal transducer and activator of transcription-y) Mol Endocrinol 2004; 18:1988–1999.
23. Herington JL, Underwood T, McConaha M, Bany BM. Paracrine signals from the mouse conceptus are not required for the normal progression of decidualization. Endocrinol 2009; 150:4404–4413.
24. Bindali, B, Kaliwal, BB. Anti-implantation activity of carbamate fungicide mancozeb in albino mice. Ind Health 2002; 40:191–197.
25. Mikel UV (ed). Advanced Laboratory Methods in Histology and Pathology. Washington, DC: Armed Forces Institute of Pathology: 1994.
26. Qi L, Anthony L, Terence J, Fordyce L, Christopher B, Elise SFA. Syntaxin 1, $G_{\alpha O}$, and N-type calcium channel complex at a presynaptic nerve terminal: analysis by quantitative immunocolocalization. J Neurosci 2004; 24:4070–4081.
27. Adams Susan M , Gayer Nalini, Terry Vera, Murphy CR. Manipulation of the follicular phase: uterodomes and pregnancy–is there a correlation? BMC Pregnancy Childbirth 2001; 1:2.
28. Kibbe WA. OligoCalc: an online oligonucleotide properties calculator. Nucleic Acids Res 2007; 35(suppl 2):W43–W46.
29. Nolan T, Hands RE, Bustin SA. Quantification of mRNA using real-time RT-PCR. Nat Protocols 2006; 1:1559–1582.
30. Hu X, Ivashkiv LB. Cross-regulation of signaling pathways by interferon-g: implications for immune responses and autoimmune diseases. Immunity 2009; 31:539–550.
31. Leiter EH. The NOD mouse: a model for insulin-dependent diabetes mellitus. Curr Protoc Immunol 1997; 24(suppl):15.9.1–15.9.23.
32. Platt JS, Hunt JS. Interferon-gamma gene expression in cycling and pregnant mouse uterus: temporal aspects and cellular localization. J Leukoc Biol 1998; 64:393–400.
33. Tan J, Paria BC, Dey SK, Das SK. Differential uterine expression of estrogen and progesterone receptors correlates with uterine preparation for implantation and decidualization in the mouse. Endocrinology 1999; 140: 5310–5321.
34. Fraser RB, Waite SL, Wood KA, Martin KL. Impact of hyperglycemia on early embryo development and embryopathy: in vitro experiments using a mouse model. Hum Reprod 2007; 22:3059–3068.
35. Seaward VC, Burke SD, Croy. BA. Interferon gamma contributes to pre-implantation embryonic development and to implantation site structure in NOD mice. Hum Reprod 2010; 25:2829–2839.
36. Raghupathy R. Th1-type immunity is incompatible with successful pregnancy. Immunol Today 1997; 18:478–482.
37. Glynn DJ, Sharkey DJ, Robertson SA. Interferon-gamma inhibits female reproductive tract responsiveness to seminal plasma. In: Proceedings of the 37th Annual Meeting of the Society for the Study of Reproduction, Vancouver, British Columbia, Canada, Aug 1–4, 2004. Biol Reprod 2004; 70(suppl 1):242.
38. Fontana V, Choren V, Vauthay1 L, Calvo JC, Calvo L, Cameo M. Exogenous interferon-γ alters murine inner cell mass and trophoblast development. Effect on the expression of ErbB1, ErbB4 and heparan sulfate proteoglycan (perlecan). Reproduction 2004; 128:717–725.
39. Cameo M, Fontana V, Cameo P, Vauthay LG, Kaplan J, Tesone M. Similar embryotoxic effects of sera from infertile patients and exogenous interferon-g on long-term in vitro development of mouse embryos. Hum Reprod 1999; 14:959–963.
40. Hunt JS, Atherton RA. Differential responses of rat trophoblast cells and embryonic fibroblasts to cytokines that regulate proliferation and class I MHC antigen expression. J Immunol 1990; 145:184–189.
41. Hibbert L, Pflanz S, De Waal Malefyt R, Kastelein RA. IL-27 and IFN-alpha signal via Stat1 and Stat3 and induce T-Bet and IL-12Rbeta2 in naive T cells. J Interferon Cytokine Res 2003; 23(9):513–522.
42. Kniss DA, Rovin B, Fertel RH, Zimmerman PD. Blockade NF-kB activation prohibits TNF-α-induced cyclooygenase-2 gene expression in ED27 trophoblast-like cells. Placenta 2001; 22:80–89.
43. Paulesu L, Jantra S, Ietta F, Brizzi R, Bigliardi E. Interleukin-1 in reproductive strategies. Evol Dev 2008; 10:778–788.
44. Dhananjaya VK. Alternate interferon signaling pathways. Pharmacol Ther 2003; 100(1):1–29.
45. Xia HF, Sun QH, Peng JP. Effect of interferon-gamma treatment on the expression of interleukin-1beta at the maternal-fetal interface of pregnant rats. Reprod Fertil Dev 2007; 19(3):510–519.
46. Geisert R, Fazleabas A, Lucy M, Mathew D. Interaction of the conceptus and endometrium to establish pregnancy in mammals: role of interleukin 1β. Cell Tissue Res 2012; (in press). Epub ahead of print March 2, 2012. DOI: 10.1007/s00441-012-1356-1.
47. Illingworth IM, Kiszka I, Bagley S, Ireland GW, Garrod DR, Kimber SJ. Desmosomes are reduced in the mouse uterine luminal epithelium during the preimplantation period of pregnancy: a mechanism for facilitation of implantation. Biol Reprod 2000; 63:1764–1773.
48. Kondo K, Kohno N, Yokoyama A, Hiwada K. Decreased MUC1 expression induces E-cadherin-mediated cell adhesion of breast cancer cell lines. Cancer Res 1998; 58:2014–2019.
49. Utech M, Ivanov AI, Samarin SN, Bruewer M, Turner JR, Mrsny RJ, Parkos CA, Nusrat A. Mechanism of IFNγ-induced endocytosis of tight junction proteins: myosin II-dependent vacuolarization of the apical plasma membrane. Mol Biol Cell 2005; 16:5040–5052.
50. Cheng JG, Chen JR, Hernandez L, Alvord WG, Stewart CL. Dual control of LIF expression and LIF receptor function regulate Stat3 activation at the onset of uterine receptivity and embryo implantation. Proc Nat Acad Sci U S A 2001; 98:8680–8685.
51. Fouladi-Nashta AA, Jones CJ, Nijjar N, Mohamet L, Smith A, Chambers I, Kimber SJ. Characterization of the uterine phenotype during the peri-implantation period for LIF-null, MF1 strain mice. Dev Biol 2005; 281: 1–21.
52. Nelson V, Davis GE, Maxwell SA. A putative protein inhibitor of activated STAT (PIASy) interacts with p53 and inhibits p53-mediated transactivation but not apoptosis. Apoptosis 2001; 6:221–234.
53. Hu W, Feng Z, Teresky AK, Levine AJ. p53 regulates maternal reproduction through LIF. Nature 2007; 450:721–72.